Separation and Purification Technology 295 (2022) 121320

Contents lists available at ScienceDirect

Separation and Purification Technology

journal homepage: www.elsevier.com/locate/seppur

Development of a novel tailored ion-imprinted polymer for recovery of lithium and strontium from reverse osmosis concentrated brine

Sara M. Alshuiael, Mohammad A. Al-Ghouti *

Environmental Science Program, Department of Biological and Environmental Sciences, College of Arts and Sciences, Qatar University, P.O. Box 2713, State of Qatar, Doha

ARTICLE INFO

Keywords:
Adsorption isotherm
Metals recovery
Ion-selective sorbents
Ion-imprinted polymer

ABSTRACT

This study aims to prepare ion-imprinted polymer (IIP) with the benefit of a metal-based sorbent, which is fabricated to selectively adsorb lithium (Li^+) from aqueous solutions, and in an attempt to remove strontium (Sr^{2+}). The adsorption processes were carried out at different pH values, initial concentrations, and temperatures, to optimize the experimental conditions, with the use of response surface methodology (RSM). The seawater reverse osmosis (SWRO) brine was physically and chemically characterized, and the physicochemical characterization of the prepared IIP before and after adsorption was also performed using different spectroscopic methods. The adsorption capacity for Li^+ and Sr^{2+} from SWRO brine was evaluated, and the reusability of IIP was investigated using adsorption–desorption cycles. The results showed that the IIP was efficient to remove Li^+ but not Sr^{2+}, and it follows Freundlich adsorption isotherms models. The analysis revealed a significant concentration of minerals in the brine sample It also revealed a low concentration of trace metals, like Ba (0.16 mg/L), Zn (0.845 mg/L), Fe (1.31 mg/L), Cu (1.165 mg/L), Pb (1.505 mg/L), and V (3.88 mg/L), except Li and Sr which shows a higher concentration of 43.32 mg/L and 16.93 mg/L respectively. pH 10 was selected to be the optimum pH for the adsorption isotherm experiments, as it was the highest efficient pH to adsorb Li^+ and Sr^{2+}. The thermodynamics study revealed that the adsorption of Li^+ on the IIP favored exothermic conditions. It was noticed that the maximum adsorption capacity (Q_m) was increased as the temperature rise from 714.3 mg/g at 25 °C to 2500 mg/g at 45 °C. The Li^+ desorption results show that 94.03% – 94.71% of the ions were recovered, while the Sr^{2+} desorption results show that 96.35% – 96.56% of the ions were recovered. The efficiency of IIP to adsorb lithium and strontium from brine shows that the adsorption removal% of Li^+ was between 84.21% and 84.68%, while the adsorption removal% of Sr^{2+} was between 3.83% and 10%. The cost analysis for IIP preparation was 2 USD/g.

1. Introduction

Seawater desalination is an effective technology that is widely used around the world to obtain fresh potable water [14]. The increased interest in seawater reverse osmosis (SWRO) desalination plants has raised concerns related to potential environmental problems. SWRO plants produce a large volume of water and a dense saline concentrate known as brine, which ends up in marine environments. High-income nations create a significant proportion of worldwide brine, just as they do with desalinated water (77.9%). It should be highlighted that those nations from both highly developed global areas, where brine output is generally lower than desalinated water production, and oil-rich Gulf countries, where thermal desalination methods with poor recovery ratios are commonly used, resulting in elevated brine output (Jones et al., 2019). Due to the potential for environmental concerns and obstacles from brine disposal, different methodological approaches for metal recovery have been studied.

Lithium recovery studies have started, however it is still in the early stages. It has been suggested that sorption, electrolysis, and nanofiltration be used [27]. Adsorption is a low-cost and ecologically beneficial way to extract metals such as Cr^{3+}, Cr^{6+}, Pb^{2+} Li^+ and Sr^{2+} from an aqueous solution [56,36,35,34] ,Gusti et al. [10]. Generally, adsorbents are not specific with little selectivity for a single metal [30], such as the commercial resins have poor selectivity. This drives the researchers to synthesize resins that have an improved property to selectively recover gold from waste [16,5,15] As a result, it is critical to develop a novel

* Corresponding author.
E-mail address: mohammad.alghouti@qu.edu.qa (M.A. Al-Ghouti).

https://doi.org/10.1016/j.seppur.2022.121320
Received 9 April 2022; Received in revised form 15 May 2022; Accepted 17 May 2022
Available online 23 May 2022

adsorbent to selectively separate lithium and strontium from an aqueous solution. The current practice used in the recovery and extraction of lithium and strontium from brines is the evaporative concentration method. Although this method is cheap, the outstanding disadvantage of this method is that the method is wasteful of water, land-intensive, and time-consuming, therefore considered an impractical method of extracting lithium and strontium from brine. This brings us to the future of lithium and strontium extraction from brine; direct lithium extraction entails plucking the lithium ions from a complex geothermal soup. Nonetheless, most of the initial studies concluded that organic ion-exchange resins denoted a comparatively low selectivity when it came to lithium ions; hence, selectivity was used in the extraction process of lithium-selective sorbents [43].

Molecularly imprinted polymers (MIPs) have drawn a lot of studies' attention in the latest years, because of their excellent features, such as constancy, cheap cost of formulation, and molecular recognition capability [12]. Ion imprinting polymers (IIPs) are comparable to molecularly imprinted polymers, however, they identify ions rather than molecules after imprinting, providing the advantages of molecularly imprinted polymers as well as a superior ion recognition capability (Otero-Romani et al., 2009). The different approaches to elaborate IIP have all been classified by Rao et al. [41] as chemical immobilization, trapping, crosslinking of linear chain polymers, and surface imprinting. The forms of IIPs might differ depending on the polymerization method. Bulk polymerization generates monolithic materials, while heterogeneous by suspension or emulsion, and homogeneous by dispersion or precipitation polymerization that generates well-defined polymer particles. A core–shell arrangement can also be used to make well-defined spherical particles. Surface imprinting, on the other hand, mostly consists of an inorganic core in core–shell IIPs [9]. IIPs have many applications like solid-phase extraction which include wastewater treatment and samples pretreatment, sensors, and IIPs membrane separation. Because IIPs have greater selectivity and adsorption efficiency than typical solid sorbents such as silica gel, activated carbon, or functionalized polymer, they are employed in SPE [19]. IIPs exhibit affinity and selectivity similar to antibodies, but they are also simple to synthesize, durable in hostile environments, and affordable to manufacture [11]. There have been several IIPs for harmful metals such as nickel, cadmium, arsenic, cobalt, lead, mercury, and selenium. In addition, in the application of sensors, the recognition element is the most important component of a sensor since it is the element in response to recognizing the targeted analytes in complicated samples and binding them. Selective chemical sensors with strong thermal, mechanical, and chemical characteristics may be made utilizing ion-imprinted polymers at a reasonable cost [40].

The lithium-imprinted polymers are prepared by polymerizing a crosslinking agent (ethylene glycol dimethacrylate), an optional co-monomer, and a lithium chelate monomer [50]. The essence of preparing lithium-imprinted polymer is that once the polymers are desorbed, it leaves imprints with the arrangement, shape, and size of binding sites meant explicitly for binding Li^+. In agreement, the United States Department of Energy report highlighted the main selectivity capabilities of Li-imprinted polymers, especially concerning brines containing other competing metal ions like K^+ and Na^+ [20]. According to the experiments, which involved a brine of 390 ppm K^+, 410 ppm Na^+, and 390 ppm Li^+ at 45 °C, 75 °C, and 100 °C, it is established that the Li-imprinted polymer had an extraction efficiency surpassing 95%.

Crown ethers (CEs) are excellent model compounds that may be used to create more complicated chemical structures. Crown ethers are particularly appealing molecules because of their unusual features, which allow for a deep investigation of interchanges that are significant in the field of analytical chemistry [32]. The macrocyclic effect is widely recognized for increasing the steadiness and metal ions selectivity combined with cyclic ligands (such as crown ethers) as compared to their equivalent open-chain equivalents. When crown ethers contain concavities of the right sizing and the right functional and cross-linking monomers, they have demonstrated great selectivity to attach to the target metal ions [31].

Crown ethers and the macrocyclic host molecule's second generation have gotten a lot of interest in recent years [28]; Büning et al., 2018). Metal ions that are inside the crown ethers have the ability to synchronize with oxygen atoms within the concavities of the crown. For stable binding and selectivity, selecting a crown ether with suitable concavities for intended ions is critical.

The latest studies have provided a detailed insight into the application and synthesis of organic polymers, which selectively extract lithium or strontium in favor of other metal ions. The ion-imprinting process is the basis of the method as it allows only lithium ions and not any competing ions to go through. Moreover, various approaches were explored to minimize the environmental effect of radionuclides. The adsorption method is the most dependable way for hazardous radionuclide removal and has been widely utilized [26]. Hence, this study aimed to explore the possibility of recovering strontium using the lithium IIP, to study if it could be used for multiple ion adsorption. The innovative objective of the project was the fabrication of imprinted polymer with the benefit of a metal-based catalyst, the elucidation of the prepared material by spectroscopic methods, and the evaluation of its adsorption capacity for Li^+ and Sr^{2+} from brine concentrate.

2. Methodology:

2.1. Chemicals

Acetonitrile (CH_3CN) (99.5%), lithium chloride (LiCl) (98%), potassium persulphate ($K_2S_2O_8$) (98%) and sodium hydroxide pellets (NaOH) (98%) were obtained from Research Lab (Mumbai, India). Ethylene glycol dimethacrylate (EGDMA) (98%, stabilized with hydroquinone monomethyl ether), dicyclohexano-18-crown-6 ($C_{20}H_{36}O_6$) (98%), hydrochloric acid (HCl) (37%), and nitric acid (HNO_3) (65%) were obtained from Sigma-Aldrich (Darmstadt, Germany). Tert-butyl acrylate ($C_7H_{12}O_2$) (99%, stabilized with 15 ppm 4-methoxyphenol) was obtained from Alfa Aesar (Heysham, England). Double deionized water was prepared in the lab using the Milli- Q® water system.

2.2. Lithium Ion-Imprinted polymer preparation (Li-IIP)

The precipitation polymerization technique was done using the method developed by Hashemi et al. [20] methodology with some modifications to prepare lithium IIP (Fig. 1). In a 50 mL glass bottle, 20 mL of acetonitrile was added with 74.5 mg of Dicyclohexano-18-crown-6 and 21.28 mg of LiCl dissolved in it for 20 min at room temperature and sonicated with an ultra-sonicator (Grant XUB series, digital ultrasonic bath). Then 792.9 mg ethylene glycol dimethacrylate (EGDMA) (Crosslinker), 128.17 mg tertbutyl acrylate (monomer), and 25 mg of potassium persulphate were mixed with the previous solution and sonicated at again 25 °C. It was then purged with N_2 for 10 min, sealed, and thermally polymerized in an oil bath at 65 °C for 24 h. Following 24 h, the polymer was filtered to discard the solvents. Then, the powder IIP was washed with methanol to remove the un-reacted materials and leached with 1 mol/L HNO_3 until the washed solution was free from lithium ions. Lastly, the lithium IIP was washed with distilled water until it reaches neutral pH. The final IIP should be fully dried.

2.3. Physical and chemical characterization of the ion imprinted polymer

The prepared ion-imprinted polymer was characterized before and after adsorption using a scanning electron microscope (SEM) (Nova™ Nano SEM 450 – FEI), transmission electron microscopy (TEM) (TEM TECNAI G2, TF20 – FEI), Fourier-transform infrared spectrophotometer (FTIR) (PerkinElmer, spectrum range: 400 cm^{-1} to 4000 cm^{-1}), and X-ray diffraction (XRD) (Empyrean XRD platform and PIXcel^{1D} detector). Specific surface area and pore size distribution were determined by

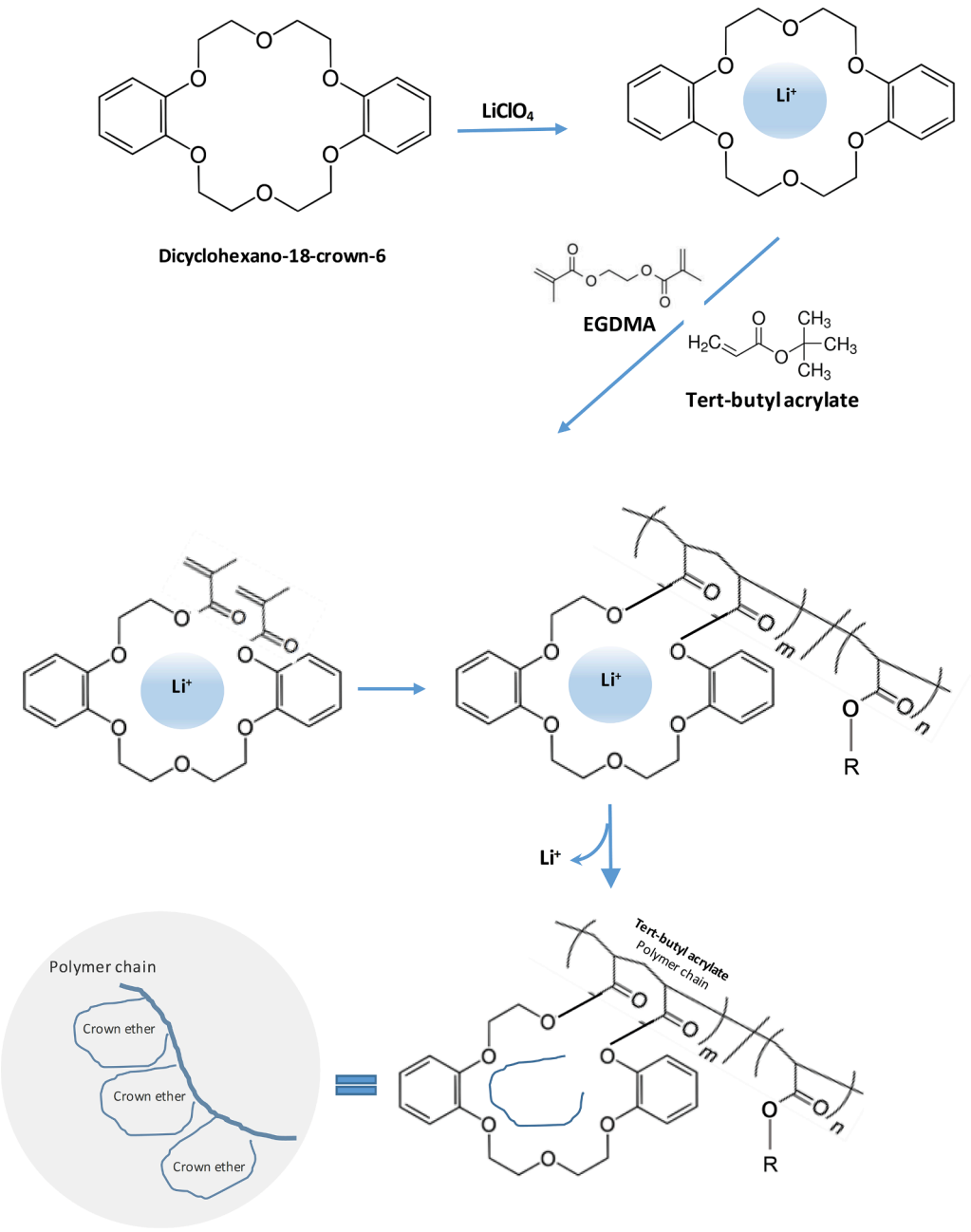

Fig. 1. Scheme of lithium ion-imprinted polymer synthesis.

Brunauer-Emmett-Teller (BET) (Quantachrome Corporation, Nova 3000). Energy Dispersive X-Ray Analysis (EDX) was also done to identify the elemental composition of the imprinted polymer, and X-ray photoelectron spectroscopy (XPS) (Ultra DLD XPS Kratos) was used to quantify the surface composition of the polymer.

2.4. Optimizing the experimental conditions and experimental design

The response surface methodology (RSM) has widely been used for optimizing a variety of waster treatment processes (Kusuma et al., 2015, 2021; [3]. The central composite design (CCD) was used to study the effects of initial concentration and temperature on the recovery of lithium and strontium.

To optimize the adsorption batch experimental conditions, stock solutions of lithium (100 ppm) and strontium (100 ppm) ions were prepared. All the experiments were run in replicates. The standard deviations of the experiments were calculated. Then, the optimized experimental conditions were applied to the real brine sample.

2.4.1. Effect of pH

To investigate the effect of pH on the adsorption processes, batch adsorption experiments were carried out at different pH values (2, 4, 6, 8, and 10). 10 mg of IIP was added to 30 mL from each different pH value with continuous shaking for 24 h, the solution was filtrated after adsorption, and both the treated solution and the IIP were preserved separately for further testing.

2.4.2. Effect of initial concentration

To investigate the effect of initial ions concentration on the adsorption processes, the stock solutions of Li^{+} and Sr^{2+} were prepared to different concentrations, namely (0 (control), 5, 15, 30, 45, 60, 75, 90, 100 mg/L). 10 mg of IIP was added to 30 mL from each diluted solution

with continuous shaking for 24 h, the solution was filtrated after adsorption, and both the treated solution and the IIP were preserved separately for further testing.

2.4.3. Effect of solution temperature

To test the effect of solution temperature on the adsorption experiment, the adsorption experiment was done at different temperatures (25 °C, 35 °C, and 45 °C). 10 mg of IIP was added to a 30 mL solution with continuous shaking in an incubator shaker (Shel-lab SSI10R-2, Orbital-Shakin) for 24 h under different temperatures, the solution was filtrated after adsorption, and both the treated solution and the IIP was preserved separately for further testing.

2.4.4. Verifying the optimized experimental conditions

The concentrations of Li^+ and Sr^{2+} were tested using inductively coupled plasma – optical emission spectroscopy (ICP-OES Optima 7300 DV – PerkinElmer) to find out the amount of lithium and strontium adsorbed under different conditions and to decide the optimum conditions for the following experiments.

2.5. Isotherm models

The experimental data is used to fit the different isotherm models using the following equations:

$$\textbf{Langmuir model}: Qe = \frac{QmbCe}{1 + bCe} \tag{1}$$

Where Q_e is the amount of metal adsorbed per gram of adsorption (mg/g), C_e is the equilibrium concentration of adsorbate (mg/l), Q_m is maximum adsorption capacity (mg/g) (constant), and b is the Langmuir constant.

$$\textbf{Freundlich model}: Qe = KfCe^{1/n} \tag{2}$$

Where Q_e is the amount of metal adsorbed per gram of adsorbate at equilibrium (mg/g), C_e is the equilibrium concentration of adsorbate (mg/L), K_F is Freundlich isotherm constant (mg/g), and n is adsorption intensity.

$$\textbf{Dubinin} - \textbf{Radushkevich model}: Qe = qse^{-K\varepsilon^2} \tag{3}$$

Where Q_e is the amount of adsorbate in the adsorbent at equilibrium (mg/g), q_s is theoretical isotherm saturation capacity (mg/g), K is adsorption energy constant, and ε is Dubinin-Radushkevich isotherm constant, which can be calculated by RT ln $[1 + \frac{1}{C_e}]$, where R is the gas constant (8.314 J/mol K), T is the absolute temperature (K) and C_e is the adsorbate equilibrium concentration (mg/l).

$$\textbf{Temkin model}: Qe = \frac{RT}{Bt}\ln(AtCe) \tag{4}$$

Where Q_e amount of adsorbate in the adsorbent at equilibrium (mg/g), C_e - equilibrium concentration of the adsorbate (mg/l), A_T - Temkin isotherm equilibrium binding constant (L/g), and B_T - Temkin isotherm constant, where R is the gas constant (8.314 J/mol K), and T is the absolute temperature (K).

To fit the isotherm equation, some parameters should be calculated by linearizing the isotherm models. To linearize the isotherm models, Table 1 is used to draw the graphs of each model. Then from the linear plotting equation, the models' parameters are calculated (Table 1).

2.6. Thermodynamics studies

Gibb's free energy (ΔG°) is a valuable indicator of impulsive behavior. If ΔG° (Eq. (5)) has a negative value at a particular temperature, a spontaneous reaction will occur. The heat of adsorption or enthalpy (ΔH°) and entropy (ΔS°) (Eq. (6)) are essential thermodynamic measurements for enthalpy and entropy variations.

Table 1
Isotherm models linearization graph axis, and calculating the model parameters from the liner plotting equation.

The Isotherm Model	**X-axis Vs Y-axis**			
Langmuir isotherm model	1/ce (x-axis) Vs. 1/qe (y-axis)			
Freundlich isotherm model	ln(ce) (x-axis) Vs. ln(qe) (y-axis)			
D-R isotherm model	e^2 (x-axis) Vs. ln(qe) (y-axis)			
Temkin isotherm model	ln(ce) (x-axis) Vs. qe (y-axis)			
Model	**Langmuir**	**Freundlich**	**D-R**	**Temkin**
Parameters	$Q_m = 1/\text{Intercept}$	$n = 1/\text{Slop}$	$q_s = e^{\text{Intercept}}$	$A_t = e^{\text{Intercept}/\text{Slop}}$
	$b = 1/\text{Slop}*Q_m$	$K_f = e^{\text{Intercept}}$	$K = \text{Slop}$	$B_t = (RT/B)$ where B = Slop

$$\Delta G^{\circ} = -RT\,lnk_L = \Delta H^{\circ} - T\Delta S^{\circ} \tag{5}$$

Where R is the universal constant 8.314 J/mol.K, T is the temperature (Kelvin), and K_L is the Langmuir isotherm constant (b).

$$lnk_L = \frac{-\Delta H^{\circ}}{RT} + \frac{\Delta S^{\circ}}{R} \tag{6}$$

Where ΔH° and ΔS° are determined from the slope and intercept of the equation of the line that is evaluated from the plot of $\ln K_L$ vs. T

2.7. Chi-Square test

The Chi-Square was calculated to find the best-fitted isotherm model, using the following equation:

$$\sum_{i=1}^{n} \frac{(q^i_{exp} - q^i_{pred})^2}{q^i_{pred}} \tag{7}$$

Where, q^i_{exp} is the adsorption capacity (mg/g) from the experimental data, q^i_{pred} is the adsorption capacity (mg/g) from the predicted (isotherm models) data, n denotes to the number of sizes which is 8, and i is the number of match experimental runs conducted to find out the adsorption capacity.

2.8. Batch desorption experiment / Adsorption-Desorption experiment

The IIP previously dried and kept from the previous isotherm experiments were used in this experiment to test the Li^+ recovery ability from IIP. The used IIP samples were washed with 10 mL of 0.5 mol/L HNO_3 with continuous shaking for 24 h at room temperature. Using ICP, the eluted ions concentrations were measured. To calculate the recovered % of ions from the IIP, first, the amount of ion adsorbed on the IIP was calculated by subtracting the final concentration from the initial concentration $(Co - Ce)$. Then the recovery % was determined as follows:

$$R\% = \frac{Elutedions\ concentration}{Co - Ce} \times 100 \tag{8}$$

A second adsorption–desorption cycle is run in the same used IIP after drying from the desorption experiment, performing the same adsorption steps as in section 2.4.2 and a second batch desorption experiment. The difference between the adsorption capacities is used to evaluate the IIP regeneration performance.

2.9. Batch adsorption experiment – Real brine sample

The following batch method was used to investigate the adsorption of Li^+ ions and the selectivity toward Sr^{2+} ions by the prepared Li^+ ion-

imprinted polymers. 10 mg of IIP was added to 30 mL brine in the batch experiment. 0.5 mol/L HNO_3 was used to keep the pH around the optimized pH. All the experiments were run in replicates.

To calculate the adsorption removal percentage of IIP to adsorb lithium and strontium ions, the initial concentration (Co), and equilibrium concentrations (Ce) will be compared as follows:

$$AR\% = \frac{(Co - Ce)}{Ci} \times 100 \quad (9)$$

The IIP particles' adsorption capacity (mg/g) in relation to the imprint metal ion will be determined as follows:

$$Qe = (Co - Ce)(\frac{V}{m}) \quad (10)$$

Where V is the volume of the brine (L), and m is the mass of the IIP used (g).

2.10. Statistical analysis

The statistical analysis was generated using MINITAB statistical analysis software. Two-way ANOVA was calculated using the temperature and initial concentration as two independent factors, to determine the significance of each factor from the P (probability) -value. Tukey grouping method with a 95% confidence level was also used to determine the significant difference between each value within the factor. Furthermore, factorial plots were drawn for Qe main factors and interaction plots to understand if the factors are dependent or independent.

2.11. Cost analysis

Cost analysis was done by breaking down the cost of the used chemicals and energy consumed as well as other extra expenses needed for the production of ion-imprinted polymers.

3. Results and discussion:

3.1. Ion-Imprinted polymer physicochemical characterization

The prepared ion-imprinted polymer was characterized using a scanning electron microscope (SEM), transmission electron microscopy (TEM), Fourier-transform infrared spectrophotometer (FTIR), and X-ray diffraction (XRD) to study the morphology of the adsorbents and their functional groups. Specific surface area and pore radius was determined by Brunauer-Emmett-Teller (BET). Energy Dispersive X-ray Analysis (EDX) was also done to identify the elemental composition of the imprinted polymer and X-ray photoelectron spectroscopy (XPS) was used to quantify the surface composition of the polymer.

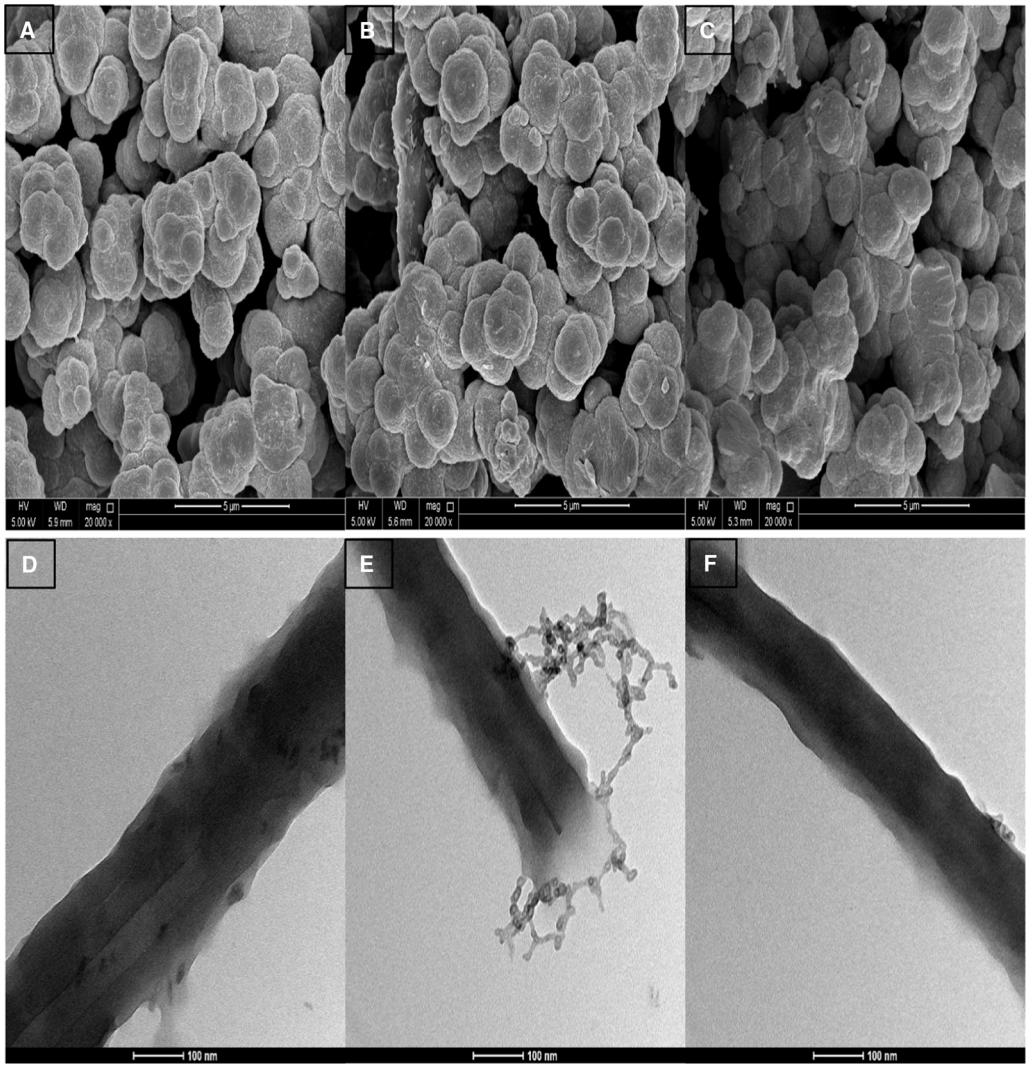

Fig. 2. (1) SEM image of IIP (A) Before adsorption, (B) After Li^+ adsorption, and (C) After Sr^{2+} adsorption. and (2) TEM image of IIP (D) Before adsorption, (E) After Li^+ adsorption, and (F) After Sr^{2+} adsorption.

3.1.1. Scanning electron microscope (SEM) and transmission electron microscopy (TEM)

The characteristics of IIPs, like other metal-ion sorbents, are closely connected to their morphology: their form and porous structure. Fig. 2 (A, B, and C) shows the SEM images of the prepared polymer before adsorption and after adsorption of lithium and strontium showing their morphology at 5 μm in 20.00 KX magnification.

The SEM scans of the polymer revealed an irregular spherical shape

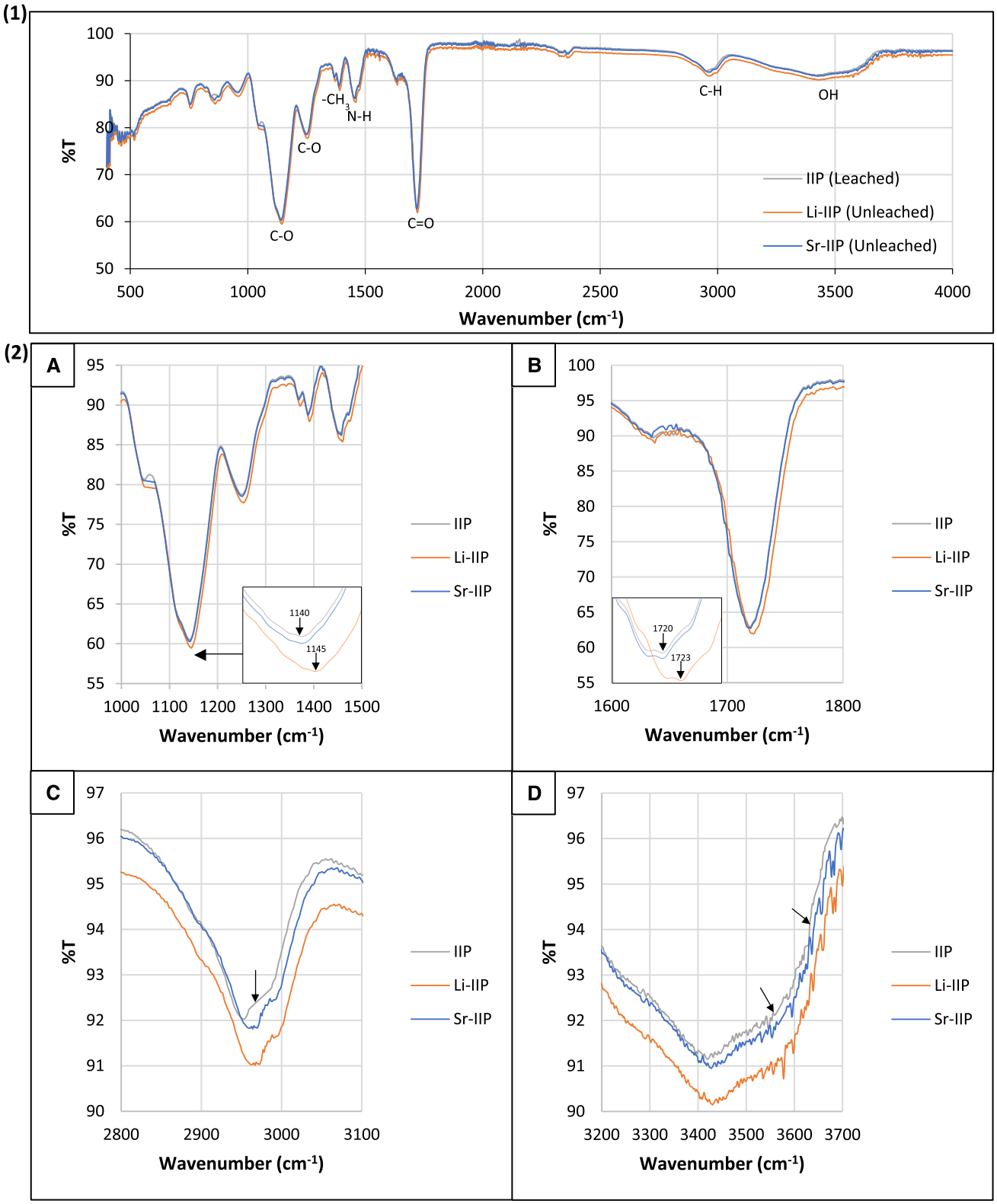

Fig. 3. (1) Fourier-transform infrared (FTIR) Spectrum of IIP, and (2) FTIR spectra sub-regions major peaks (A) fingerprint region 1000 cm^{-1} to 1500 cm^{-1} (B) double bond region 1500 cm^{-1} to 1800 cm^{-1}band (C) C-H (Aliphatic) strong alkane stretch 2800 cm^{-1} to 3100 cm^{-1} and (D) Normal "Polymeric" OH stretch 3200 cm^{-1} to 3700 cm^{-1}.

polymer with a very regular porous and consistent surface structure of the IIP, with a rough and mound surface. On the surfaces of the polymers, there exist local pores, which are evenly dispersed. It is noticed that the leached IIP has a rough and porous surface, which indicates empty binding sites for the target ions with an increase in the surface area to improve the adsorption and facilitate the capture of targeted ions. The removal of the template ion increases the roughness of the surface of the imprinted polymer [9]. Long et al.)2016) refer that the polymer particles have a spherical shape because of the mechanism of precipitation polymerization. In addition, Xu and Guo [51] explain that the porous texture aids in increasing the adsorption of the superficial area and exposes the surface binding sites.

The BET results show that the multi-point specific surface area (SSA) is 40.80 m^2/g and Barrett–Joyner–Halenda (BJH) adsorption average pore radius is 4.83 nm. Compared to Al-Ajji and Al-Ghouti [2] hazelnut shell adsorbent with 3.7 m^2/g SSA and 50.6 nm pore radius size, it can be noticed that the IIP had more than 10 times larder SSA with pore radius sizes that are smaller by more than 10 times. This indicates that the IIP is highly porous with small pores that increase the surface area and roughness of the surface. On the other hand, copper IIP has 93.2 m^2/g SSA and a 9.5 nm pore radius size [51], which is double the Li IIP values. This could be due to the fact that Li^+ is much smaller than Cu^{2+}, which in consequence will have an effect on the IIP structural sizes while preparing it using the ion templets. This fact was also shown in the cobalt IIP and nickel IIP, where the IIPs had 74.94 m^2/g and 89.04 m^2/g SSA and 9.3 nm and 12.4 nm pore radius size respectively [54,53] . This could be a result of the fact that both Co^{2+} and Ni^{+2} are also bigger than Li^+, where they have almost the same size as Cu^{2+}.

The SEM images show a significant difference in morphology observed between the leached IIP and unleached IIP. The lithium adsorption on IIPs causes a visual change in the surface structure (Fig. 2B), while strontium adsorption SEM images and the leached IIPs are similar to each other in the context of the polymer surface roughness. The adsorption of lithium as a target ion used in the polymerization can be the cause of the morphological variations between them.

Unleached Li-IIPs reveal more than the target ion, which is bonded evenly in SEM images. Due to the bounded lithium ions, a rough and aggregated structure was seen on the surface of unleached IIPs [23]. Because leached IIPs are the results of cross-linking and imprinting processes, which increase the adsorption surface area and provide open areas on the surface permitting binding, there are numerous micropores on the surface of leached IIPs, allowing the target ion to bind readily [23].

To investigate the microstructure of the IIP, a further step was taken by using the TEM. Fig. 2 (D, E, and F) shows the TEM image of the pure IIP before adsorption, and after adsorption of Li^+ and Sr^{2+}. As in the SEM image, the TEM image of IIP after strontium adsorption and the pure IIP TEM image are similar to each other, and nothing major is observed. While the after Li^+ adsorption IIP TEM images (Fig. 2(1)E) can clearly show the adsorption of the lithium ions in a multilayer behavior with the interaction between the ions. This indicates that Freundlich isotherm adsorption behavior is expected.

3.1.2. Fourier transform infrared spectroscopy (FTIR)

The prepared ion-imprinted polymer was characterized using FTIR to study the adsorbent functional groups. Fig. 3 (1) shows the FTIR spectra were the adsorption due to C–O stretch (alkyl-substituted ether) (1140 cm^{-1}), C–O bend (aromatic ethers) (1250 cm^{-1}), $–CH_3$ (methyl) (1390 cm^{-1}), N-H stretch (Amide) (1459 cm^{-1}), C = O stretch (Carbonyl) (1720 cm^{-1}), C–H (aliphatic) strong alkane stretch (2993 cm^{-1}), and normal "polymeric'' OH stretch (broad) (3400 cm^{-1}) were observed.

The prepared Li^+ ion-imprinted polymer's FTIR spectra results were compared with the Li^+ ion-imprinted polymers prepared by Hashemi et al. [20]. The spectrum shows closely similar functional groups, where they contain C = O stretch, C–O stretch, C–O bend, C–H stretch, $–CH_3$ bend, and N-H stretch.

According to Işıkver and Baylav [23], the strong C–O stretching band at 1150 cm^{-1} appears because of the monomers in the polymeric structure bearing –COOH groups. It was also recognized that the C–H strong alkane stretching band at approximately 2950 cm^{-1} wavenumber was identified in all-metal ion-imprinted polymers, which was observed in the prepared IIP at wavenumber 2993 cm^{-1} This accentuates the presence of the C–H group in the group polymers at this wavenumber. Moreover, strong carbonyl C = O stretching and N–H strong amide stretching bands were also found in all the polymers [23].

Hashemi et al. [20] study compared the unleached and the leached ion-imprinted polymer FTIR spectra. The comparison shows that the leaching process does not affect the functional groups of the IIP, suggesting that the IIP is reproducible. In addition, in Işıkver and Baylav [23] experiments, they compare the leached IIP and the control polymer spectra, it was found that they show a similar spectrum, which indicates that the leaching process is considered to cause no damage to the polymer network while removing the ions. This explains the fact that the spectrum of the IIP before adsorption (leached) and after adsorption of Li and Sr (unleached) were similar.

A close interpretation of the spectra (Fig. 3(2)) revealed that there are not many differences between the spectral features and the functional groups of the IIP before adsorption and after adsorption. However, there are some changes in the transmittance percent of few bands as well as some slight shifts in the exact position of the bands, which was noticed mostly in the after Li^+ adsorption IIP. This change proposes that the structure of the IIP shows the effects on the exact position of the bands and shifts in the bands when the internal structure is changed while capturing the Li^+ ions.

The FTIR are generally sub-divided to four main region including: fingerprint region (500 cm^{-1} to 1500 cm^{-1}), double bond region (1500 cm^{-1} to 2000 cm^{-1}), triple bond region (2000 cm^{-1} to 2500 cm^{-1}) and single bond stretch region (2500 cm^{-1} to 4000 cm^{-1}). Fig. 3(2) shows a zoomed view of the major peaks in each region. It was noticed generally that the FTIR after Li^+ adsorption is obviously different from the IIP before adsorption and IIP after adsorption of Sr^{2+}. This indicates that the IIP after Sr^{2+} adsorption is actually rarely adsorbing an ion, which means that the binding sites are still empty as much as it was before adsorption. This supports the theory that the IIP was designed with a templet of lithium ions to be selective for lithium recovery. In the fingerprint region (Fig. 3A) and the double bond region (Fig. 3B), it was observed that the after Li^+ adsorption peaks were shifted. The C-O stretch peak at 1140 cm^{-1}, which appears because the monomers in the polymeric structure bearing –COOH groups were shifted from 1140 cm^{-1} before adsorption to 1145 cm^{-1}, and it was wider and less transmitted. This could be due to the interaction of the lithium ions with the monomer when it was captured in the binding sites. The carbonyl C = O stretch at 1720 cm^{-1} was also wider, less transmitted, and shifted from 1720 cm^{-1} before adsorption to 1723 cm^{-1} after Li^+ adsorption. In the case of the C–H (Aliphatic), strong alkane stretch (2993 cm^{-1}), and Normal "polymeric'' OH stretch (3400 cm^{-1}) were observed. After Li^+ adsorption peaks are still less transmitted and wider, but it was also noted that the peaks of the IIP before adsorption are smothered than the peaks after adsorption of both Li^+ and Sr^{2+}, and the after Sr^{2+} adsorption peaks are a bit wider than the peaks before adsorption. This is due to the fact that there is adsorption even if it is a small quantity, which indicates that this small quantity affects the single bonds in opposite to the other bonds.

3.1.3. X-Ray diffraction (XRD), energy Dispersive X-Ray (EDX), and X-ray photoelectron spectroscopy (XPS).

To evaluate the existence or absence of lithium and strontium ions in the ion-imprinted polymer matrix before and after adsorption, different kind of X-ray spectroscopy analysis (X-ray diffraction (XRD), energy dispersive X-ray (EDX), and X-ray photoelectron spectroscopy (XPS)) was investigated.

In the first X-ray spectroscopy analysis, the XRD diffractogram of the

IIP (Fig. 4(1)) shows similar patterns before and after adsorption, except for a few peaks at 2θ = 32.67, 36.15, 51.55, and 64.82°. These intense diffracted peaks in the after Li^+ adsorption pattern are corresponding to lithium, which indicates the adsorption of the lithium ions on the IIP. Trivedi et al. [45] studied the properties of the lithium powder. The XRD diffractogram of lithium samples shows peaks at 2θ = 32.67, 36.15, 52.16, 64.56, 64.84, and 65.02°, this confirms that the intense peaks are a result of the presence of lithium in the sample. In addition, as these peaks are not shown in the leached IIP, this insure that the lithium ions used as a template in the preparation steps of the IIP were completely washed off leaving available imprinted sites for lithium. Moreover, there is a small intense peak at 2θ = 31.08°in the after Sr adsorption

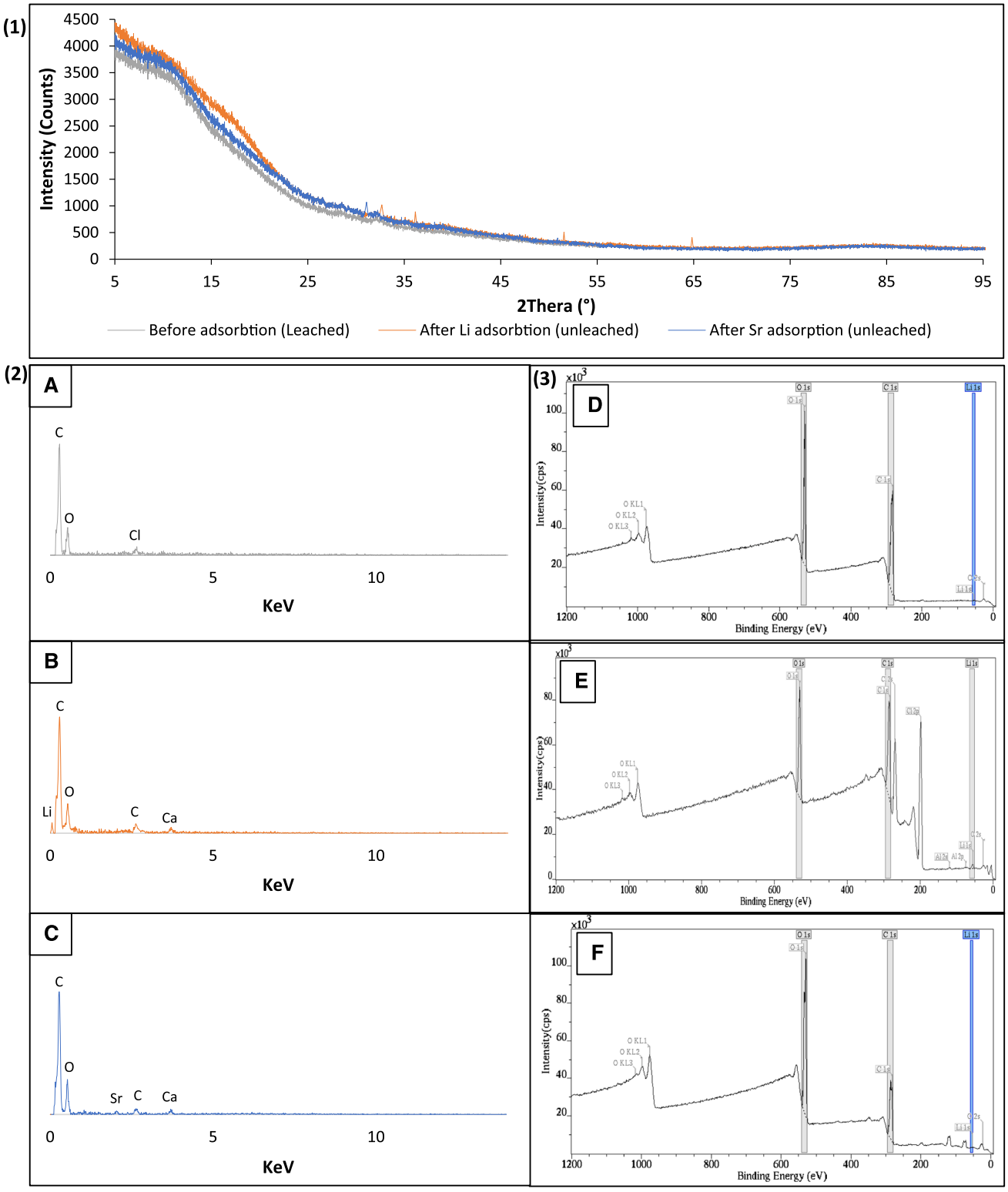

Fig. 4. (1) XRD diffractogram of IIP before adsorption and after adsorption, (2) EDX spectra of IIP: (A) Before adsorption, (B) After Li^+ adsorption, and (C) After Sr^{2+} adsorption, and (3) XPS spectra of IIP (D) Before adsorption, (E) After Li^+ adsorption and (F) After Sr^{2+} adsorption.

diffractogram, this can be corresponding to the small amount of strontium adsorbed by the IIP. Boanini et al. [8] analyzed the XRD pattern of strontium in a study comparing strontium and zinc substitution in β-tricalcium phosphate. They found that the strontium showed a very intense peak at 2θ around 31°. This agreed that the diffracted peak at 31.08 is corresponding to strontium.

The characterization of metal ion-imprinted polymers using XRD was done by Işıkver and Baylav [23] for the nickel IIP and cobalt IIP experiments and in Behbahani et al. [6] for the nickel nanostructured IIP. In all of those metal ion-imprinted polymers, the XRD pattern of the leached and unleached IIP was similar except in a few peaks corresponding to the metal used in the IIP preparation. Moreover, it can be noticed that the ion-imprinted polymers generally show closely similar XRD diffractogram that is highly zigzag due to the polymer's amorphous nature [23].

Moreover, when the material is more amorphous it shows higher diffraction intensity [52], this can explain the fact that it can be noticed that the IIP before adsorption has a higher intensity, followed by the IIP after Sr^{2+} adsorption, then the IIP after Li^{+} adsorption. This is mainly because the IIP before adsorption has a more imprinted binding site and is rougher as shown before in the SEM surface image. The IIP after Li^{+} adsorption is smother, as the Li^{+} occupy most of the imprinted binding sites, and the IIP after Sr^{2+} adsorption is just in between both of them, as the IIP was designed to selectively adsorb lithium ions, but this did not eliminate the fact that some other ion can be adsorbed rarely.

In the second spectroscopy analysis, the EDX spectrum of the IIP before adsorption (Fig. 4(2)A) shows that the IIP is composed mainly of carbon, oxygen, and a trace amount of chloride. The element composition weight percentage in Table 2 shows that 73.27% of the IIP is composed of carbon, 25.30% is composed of oxygen and the other 1.43% is chloride. It is noticed that the ion-imprinted polymer is totally free of lithium, which indicates that the lithium was leached perfectly, while a small amount of chloride was indicated, which is most probably due to the lithium chloride used to prepare the IIP.

The EDX spectrum after lithium adsorption (Fig. 4(2)B) shows a good peak corresponding to lithium in the composition of the IIP, indicating successful lithium adsorption. On the other hand, the EDX spectrum after strontium adsorption (Fig. 4(2)C) shows a very small peak corresponding to strontium, which means that the IIP was not able to adsorb strontium with the same efficiency as adsorbing lithium. In addition, it was observed that there is a peak corresponding to calcium in the after adsorption spectra, this could be due to a random error in the used distilled water purification system, which leads to the availability of calcium ions as a competitor to be adsorbed.

Branger et al. [9] mentioned the use of EDX spectroscopy to analyze polymers used to adsorb Cu(II) ions before and after extraction. It was stated that the EDX is capable to show the ions in the surface and the core of the polymer, and their results show a clear decrease in the Cu(II) ions composition after leaching it from the polymer particles. Also, in an experiment to selectively remove Cr(VI) using IIP grafted on the electrospun nanofibrous mat of functionalized polyacrylonitrile (FPANFM) [21], the EDX spectroscopy analysis was used. It was characterized the composition of the IIP before and after the removal of the Cr(VI) ions, but it was further employed to verify the existence of the FPANFM structure in the IIP to confirm the successful preparation of IIP-functionalized-PANFM. Liu et al. (2015) also used the EDX to confirm the successful imprint of the nickel in the ion-imprinted polymer while preparing it based on graphene oxide/SiO_2

In the third spectroscopy analysis, the XPS spectrum of the IIP before adsorption (Fig. 4(3)D) shows that the IIP is composed mainly of carbon and oxygen. The XPS surface quantification of the IIP is shown in table 2. The mass concentration shows that 69.96% of the IIP is composed of carbon, 29.28% is composed of oxygen and the other 0.76% is lithium. It is noticed that even though, there is no peak corresponding to lithium in the XPS spectrum, it was detected in the surface quantification. This could be a leftover that was not totally leached while preparing the IIP. It was a very trace percentage, which is acceptable.

After lithium adsorption, the XPS spectrum (Fig. 4(3)E) shows a peak corresponding to lithium in the surface composition of the IIP, assuring that the lithium was efficiently adsorbed. On the other hand, the XPS spectrum after strontium adsorption (Fig. 4(3)F) is not showing any peak corresponding to strontium, which means that the IIP was not able to adsorb strontium in a detectable amount, as the XPS cannot detect anything less than 1% mass concentration.

Long et al.)2016), in their IIP preparation for the removal of nickel, used XPS to observe the adsorption mechanism by detecting the changes in the IIP composition before and after the adsorption of nickel. XPS was also done before leaching and after leaching in an IIP experiment that was prepared to selectively remove bromine ions [49,48]. Their results showed that bromine was found in a trace amount after leaching it from the IIP, revealing that roughly all of the imprinting sites on the surface of polymers were successfully imprinted, and polymer leaching was successful. The negligible quantity of bromine that persisted in the polymer after leaching was attributable to the fact that a tiny fraction of the imprinted sites were thoroughly buried during the imprinting process, and leaching of these remaining bromine ions was challenging under the leaching conditions.

Overall, all of the three X-ray spectroscopic analyses gave the same conclusion that the IIP before adsorption was perfectly leached from almost all of the Li ions templates while preparing it and it shows superior selective adsorption of lithium while the strontium adsorption was weak. The IIP composition results from the EDX and the XPS were very close to each other, highlighting that it is mainly composed of carbon and oxygen.

3.2. Sea water reverse osmosis brine characterization

Seawater reverses osmosis concentrated brine from desalination plant was physically and chemically characterized, where pH, salinity, total dissolved solids (TDS), conductivity, and elemental composition were tested. Table 3 shows the physical and chemical characteristics of the seawater reverse osmosis (SWRO) brine in comparison with other SWRO brine characteristics from the literature. The pH of the brine used in the current study is closer to 8, which indicates that it is alkaline. This is similar to the other brine results, where all of the pH values are

Table 2
EXD element composition and XPS surface quantification of the IIP.

Element	Mass Conc. %	Atomic Conc. %
EXD element composition		
C	73.27	79.00
O	25.30	20.48
Cl	1.43	0.52
Total	100.00	100.00
XPS surface quantification		
C	69.96	75.02
O	29.28	23.58
Li	0.76	1.40
Total	100.00	100.00

Table 3
Physical and chemical characteristics of SWRO brine.

pH	Salinity (ppt)	TDS (g/L)	Conductivity (mS/cm)	Reference
7.89	61.7	67.64	91.56	current study
8.2	39.2	NR	NR	[18]
10	NR	69.17–72.36	88–132	[7]
8	NR	30.73	77	[38]
8.17	NR	71.827	11.204	[42]
8–8-12	NR	58.85	NR	[33]

between 8 and 12 indicating that all the brine water is alkaline ranging from weak to strong alkalinity. The salinity of the brine water was 61.7 ppt. It was noticed by Khan et al. [24] that the salinity of the brine was more than 160% higher than the seawater standard salinity. The conductivity of the SWRO brine was 91.56 mS/cm. Conductive ions are generally made up of dissolved salts and inorganic elements such as chloride, alkalis, sulfides, etc. [55]. As a result, a high water conductivity is a result of a high ion concentration. Thus, as the principal charge carriers in brine are Na and Cl, it is obvious to find that the conductivity of the brine is high, as the elemental analysis of the brine (Fig. 5) shows that Na and Cl are available in high quantities in the brine water.

The elemental analysis of the seawater reverse osmosis brine is shown in Fig. 5. The analyzed trace metals include copper (Cu), zinc (Zn), iron (Fe), sodium (Na), potassium (K), magnesium (Mg), calcium (Ca), barium (Ba), strontium (Sr), lithium (Li), lead (Pb), and vanadium (V). The analysis revealed a significant concentration of minerals in the brine sample like Na (30575 mg/L), Mg (2757 mg/L), K (1700 mg/L), and Ca (1690 mg/L). It also revealed a low concentration of trace metals in the analysed brine sample, like Ba (0.16 mg/L), Zn (0.845 mg/L), Fe (1.31 mg/L), Cu (1.165 mg/L), Pb (1.505 mg/L), and V (3.88 mg/L), except Li and Sr which shows a higher concentration of 43.32 mg/L and 16.93 mg/L respectively. The chemistry of brine, the desalination process utilized, as well as the chemicals used, and the geological context of the region all impact the concentration composition of trace metals in brine [29].

As noticed that strontium and lithium are present in a higher concentration. This can be due to the presence of carbonates in the brine, chemical and physical weathering, as well as the leaching of rocks and soils. These can all contribute to strontium's higher concentrations [39], and the comparatively high proportion of lithium in brine, assures the fact that seas are key lithium reservoirs across the world [42].

3.3. Effect of pH

pH is among the most pertinent factors impacting the adsorption rate of various metal ions on the polymers.Different pH values between pH 2 and pH 10 were used to study the behavior of the ion-imprinted polymer when the pH is changed. The experiment results show that the adsorption removal percentage of lithium (Fig. 6A) ranged between 98.6% and 99% with a difference of 0.4% between the highest and lowest adsorption removal percentage. On the other hand, the adsorption removal percentage of strontium (Fig. 6B) was more irregular, ranging between 2% and 99% with no regular trend. So, pH 10 was selected to be the optimum pH for the experiments, as it was the highest efficient pH to adsorb Sr^{2+}, and in the case of Li^{+} adsorption, there was no big difference between pH 10 and the highest adsorption removal percentage (0.4%).

Işıkver and Baylav [23] in their IIP experiment investigated the effect of pH on five different pHs from 3 to 7. Their results show that the higher the pH, the higher the adsorption. They justify this phenomenon as that the polymers having –COOH groups get ionized when pH rises, resulting in increased interactions with metal ions. Moreover, the tendency for metal ion–HQ complex formation increases as pH rises. Behbahani et al. [6] in their nano IIP also tested different pH values. They also found that the adsorption raised with the pH raising from 2 to 8. They also noticed that the quantitative retention of the sorbent was reduced by reducing the pH value of the solution due to electrostatic repulsion of the protonated active sites of the sorbent with the positively charged metal species.

[37], 2018) studied the Cr (IV) removal by different adsorbents. The point zero of charges (pH_{ZPC}) for the adsorbents were 2.2 and 2.5, and the optimum pH was occurring at 2. However, this is not always correct. Kuncoro et al. [25] investigated the Cd^{2+} and Pb^{2+} adsorption by adsorbent from a mixture of the bagasse-bentonite, where the pH_{ZPC} was 7.63, while the optimum pH of the adsorption process was 5.

3.4. Effect of temperature and initial concentration

The second factor affecting the metal ion adsorption is the temperature and the metal ion's initial concentration. Thus, three experiments were run in parallel, each at a different temperature at 25 °C, 35 °C, and 45 °C. In each experiment, eight different initial concentration (5, 15, 30, 45, 60, 75, 90, and 100 ppm) was used for both lithium and strontium, and all the solutions were adjusted to pH 10. The results in Fig. 7A show that as the initial concentration of Li^{+} increase, the adsorption capacity of the IIP increase, this shows a positive correlation between the Li^{+} concentration and the adsorption capacity. Huang and Wang [22] recovered lithium ions using IIP loaded on pre-treated vermiculite. They found that the adsorption curve is directly proportional to the Li^{+} initial concentration, regardless of the changes in the adsorption time or the monomer dosage ratio. This was also observed by Luo et al. [31] in their experiment, it was established that the adsorption capacity is directly proportional to the concentration of the Li^{+} ions, for a 2.5 mmol/L – 45 mmol/L concentration range.

Unlike the Li^{+} adsorption, the Sr^{2+} adsorption (Fig. 7B) did not show a linear correlation between the initial concentration and the adsorption

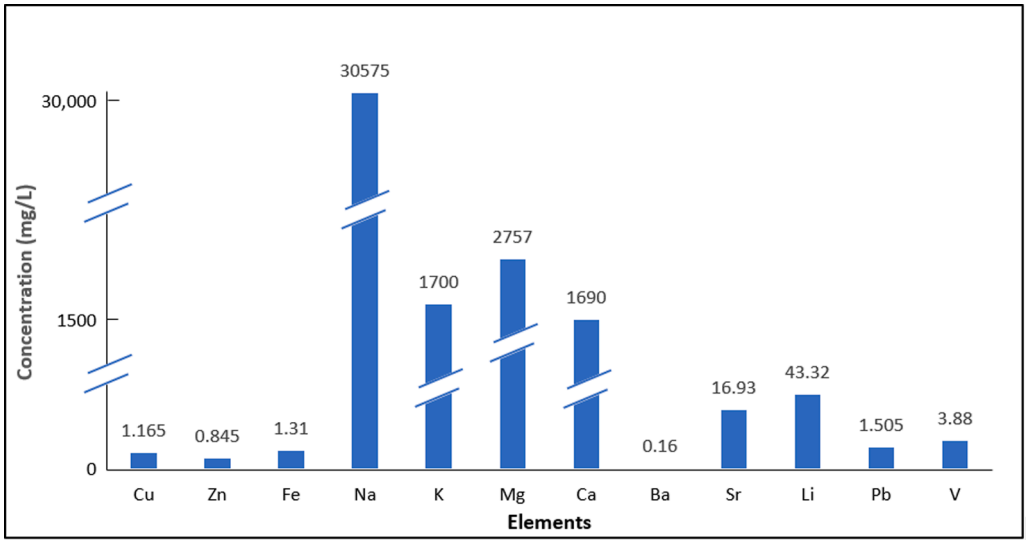

Fig. 5. Elemental compositions of the SWRO brine according to ICP-OES analysis.

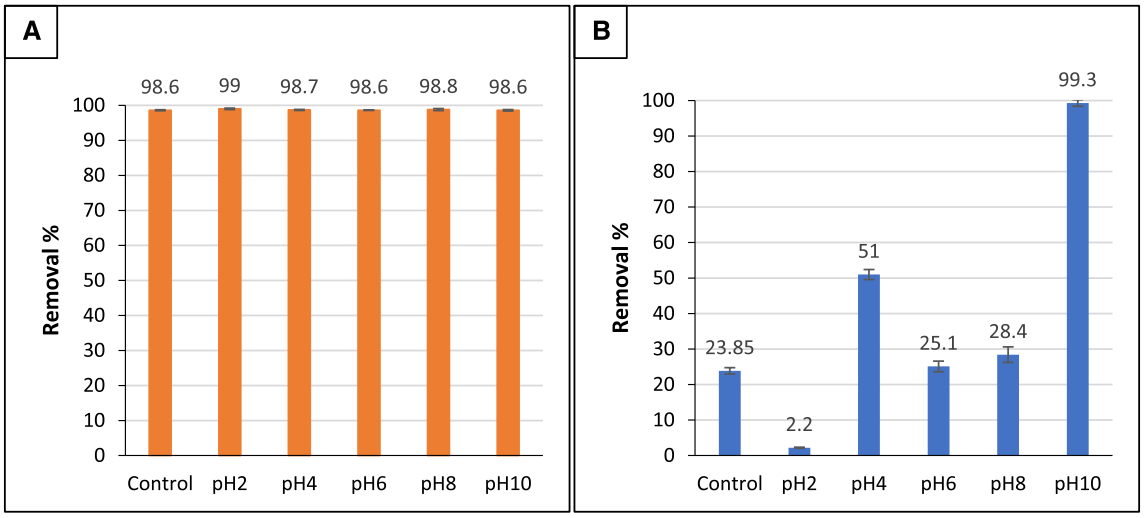

Fig. 6. Effect of pH on the IIP adsorption removal % toward (A) Lithium and (B) Strontium, at 25 °C temperature.

capacity of IIP, this was expected as the ion-imprinted polymer was tailored to have selectivity toward Li^+ only and not for Sr^{2+}. This means that the Sr^{2+} uptake is not consistent and it could be adsorbed at different temperatures and concentrations. Işıkver and Baylav [23] described this as a memory effect of the adsorbate ion with the adsorbent in the imprinting process of the polymer; this is due to the fact of strong intermolecular interaction of the imprinted polymer and the used templet.

Fig. 7(C and D) also shows the influence of temperature on the adsorption capacity of IIP on Li^+ and Sr^{2+}. In general, the increase in temperature also increased adsorption capacity. For example, at 45 °C the highest equilibrium concentration was 3 mg/L of Li^+, as compared to 3.2 mg/L of Li^+ at 25 °C and 3.67 mg/L of Li^+ at 35 °C, which means that less concentration of Li^+ is left unadsorbed at 45 °C. According to Al-Ajji and Al-Ghouti [2], an increase in adsorption capacity can be due to the increase in the diffusion rate of the adsorbate molecules due to the decrease in solution viscosity. Additionally, an increase in temperature also influences the biosorption activity by increasing the kinetic energy of the solute as well as the surface activity. Furthermore, it is also possible that high temperatures increase the flexibility of the crown of the imprinted polymer, allowing more ions to reach the binding site, but it should be noticed that all of the temperatures were giving almost the same effect and the difference was not significant. On the other hand, strontium adsorption is irregular, this can be a result of the expansion behavior of the crown, which allows the strontium ion to get into the binding site when it expands, but it will not be stably bound for a long time, as it cannot fit properly, which then will be desorbed again.

Furthermore, response surface methodology (RSM) was used to optimize the conditions of Li^+ and Sr^{2+} adsorption onto IIP at pH 10. The RSM graphical illustration (Fig. 7(E and F)) analyzes the interactions between the independent factors (initial concentration (mg/L) and temperature (^oC)) and response (adsorption capacity (mg/g)). The results showed that the optimum conditions for Li^+ adsorption are at 42.07 °C and an initial concentration of 86.09 mg/L, which resulted in 250 mg/g adsorption capacity with 0.858 desirabilities. On the other hand, the optimum conditions for Sr^{2+} adsorption were at 35.40 °C and an initial concentration of 60.12 mg/L, which resulted in 58.73 mg/g adsorption capacity with 0.867 desirabilities. The overall outcome shows that for Li^+, the model was significant but for Sr^{2+} it was not.

For Li^+ : Adsorption capacity = $-6.52010 \times 10^{-003} + 0.012037 \times$ Temperature + $2.89815 \times$ Concentration

For Sr^{2+}: Adsorption capacity = $-251.95043 + 14.52656 \times$ Temperature + $1.78299 \times$ Concentration + $6.22105 \times 10^{-003} \times$ Temperature $\times$ Concentration $- 0.21047 \times$ (Temperature)^2 $-0.016666 \times$ (Concentration)^2

3.5. Isotherm Models, Chi-Square Test, thermodynamics Studies, and adsorption mechanism

The IIP adsorption data was used to observe which isotherm model is the best fit for each temperature. As mentioned in section 2.5, the isotherm models were first linearized as shown in Fig. 8(1), and then the parameters for each temperature were calculated in table 4 using the values of the linear plotting equation of the graphs.

Langmuir isotherm refers to homogenous adsorption on the adsorbent surface and only a monolayer of adsorbate is formed on the adsorbent surface, which means that no interaction happens among the adsorbate molecules on the adsorbate surface. The correlation coefficient (R^2) of the Langmuir isotherm at the different three temperatures was 0.99, which is so close to 1, indicating that the experiment could be explained as a Langmuir isotherm. Moreover, the maximum adsorption capacity (Q_m) was rising as the temperature rise from 714 mg/g at 25 °C to 2500 mg/g at 45 °C. Likewise, the Freundlich isotherm R^2 values at the different three temperatures were also 0.99, adding the possibility that the experiment could be explained as a Freundlich isotherm. Contrary to Langmuir, Freundlich suggests that heterogeneous adsorption takes place and forms a multilayer adsorbate on the adsorbent surface, due to interactions among the adsorbate. Moreover, Freundlich adsorption capacity (K_f) was also rising as the temperature rise from 89.14 $(mg/g)/(g/L)^{1/n}$ at 25 °C to 97.55 $(mg/g)/(g/L)^{1/n}$ at 45 °C. Dubinin-Radushkevich and Temkin were not a favorable model to describe the adsorption behavior of the IIP, as the R^2 values were much lower than Longmire and Freundlich, ranging between 85 and 89. Branger et al. [9] mentioned the possibility that IIP adsorption could follow Langmuir and Freundlich models, where it is capable to have the IIP heterogeneous characteristics along with the saturation behavior at high concentrations. This model was employed in Fasihi et al. [17] uranyl IIP adsorption isotherm and Daniel et al. [13] palladium (II) IIP. However, nowadays, this model is less popular than Langmuir and Freundlich's model independently.

Fig. 8(2) shows the experimental data and the different models plot fitting at each temperature. It can be observed that the Freundlich model fits the experimental data perfectly in all of the different temperatures used, unlike Langmuir and Temkin models. This indicates that the binding sites are following heterogeneous adsorption of the adsorbate onto the adsorbent, and suggests that the IIP adsorption behavior is multilayer adsorption, where the Freundlich model does not have the restriction of the monomolecular layer. This was expected from the TEM

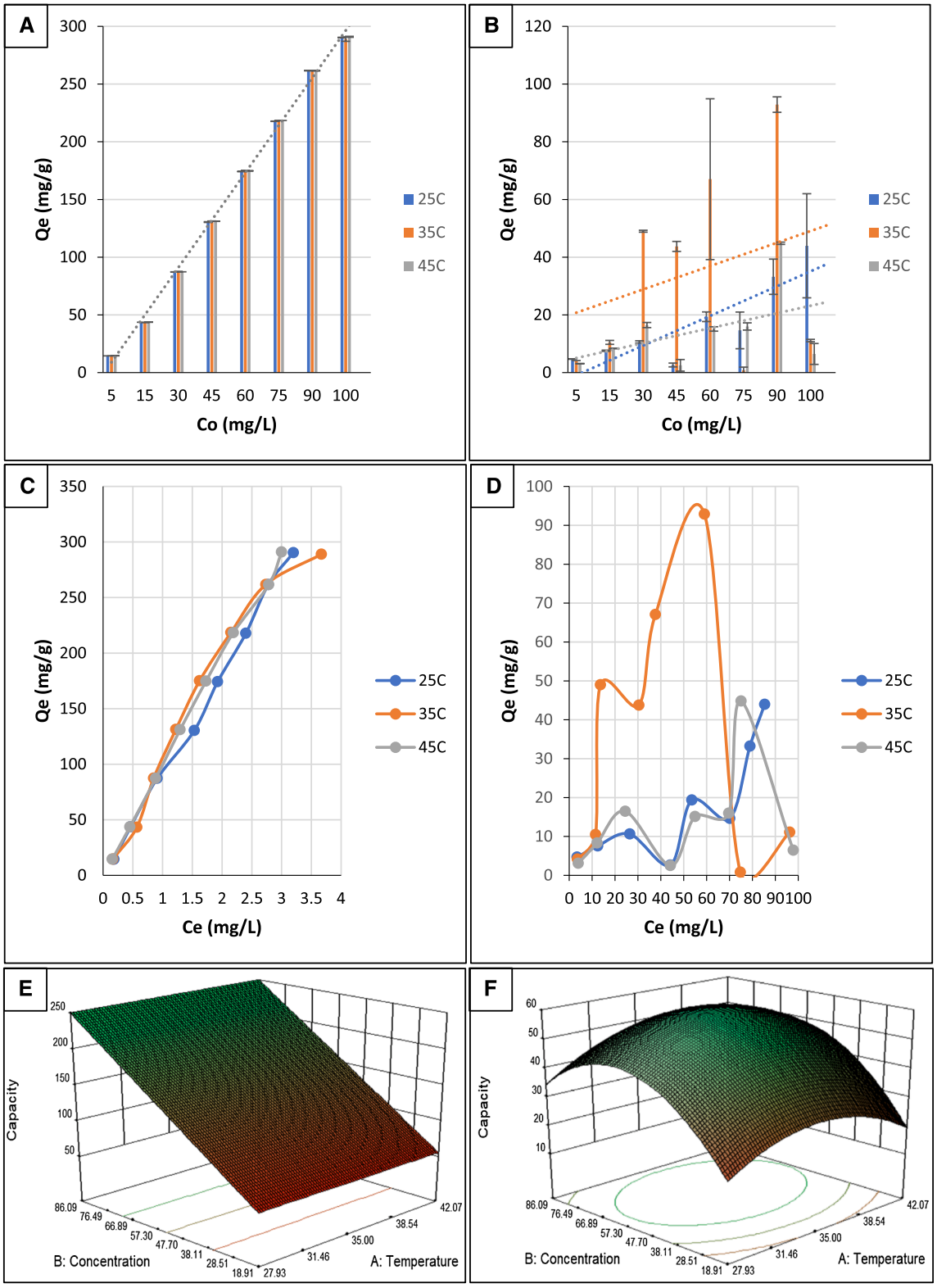

Fig. 7. Effect of initial concentration on the adsorption capacity of the IIP toward (A) Lithium initial concentration and (B) Strontium initial concentration; the correlation between the IIP adsorption capacity and equilibrium concentration of (C) Lithium and (D) Strontium at pH 10 and 25 °C, 35 °C, and 45 °C temperature; and Response surface plots of initial concentration (mg/L) and temperature (°C) for (E) Lithium adsorption and (F) Strontium adsorption onto IIP at pH 10.

image (Fig. 2E) in section 3.1.1, where it was shown that the lithium ions were aggregated on the IIP in multilayers. It must be brought that the Dubinin-Radushkevich model was not feasible to be fitted in the graphs, which excludes its applicability to be the followed model.

The lithium IIP that was prepared by Huang and Wang [22] was following the Langmuir model more than Freundlich and Temkin, indicating that it had a homogeneous binding site and behave as a monolayer adsorbent. However, their polymer was loaded on pre-treated vermiculite, which could be the reason behind the differences in the adsorption behavior. On the other hand, an IIP selective for Br(I)

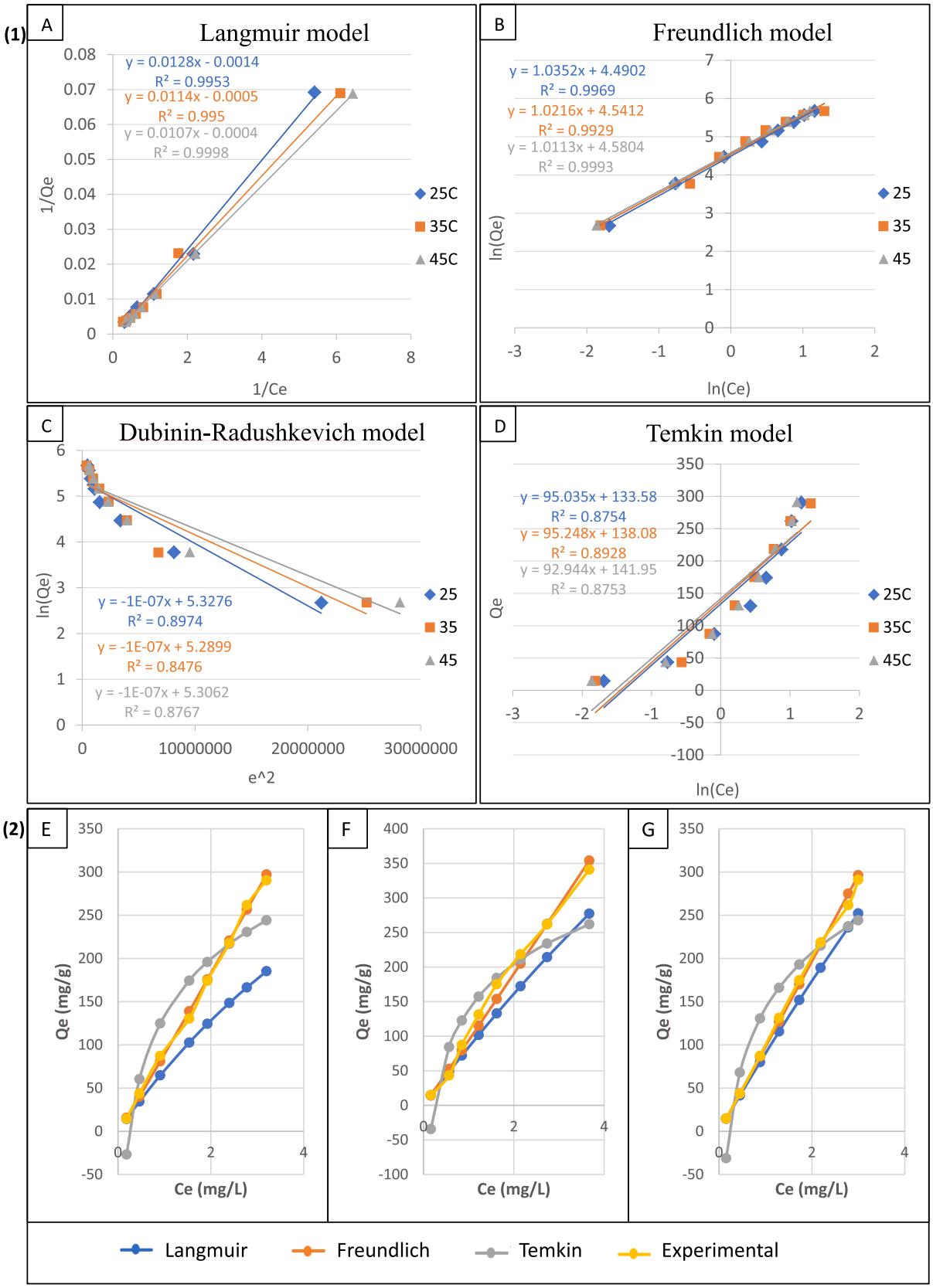

Fig. 8. (1) Linearizing graph for the isotherm models under different temperatures (A) Langmuir (B) Freundlich (C) D-R and (D) Temkin model, (2) IIP adsorption isotherm at (E) 25 °C (F) 35 °C (G) 45 °C, and (3) Li^+ Adsorption mechanisms of IIP.

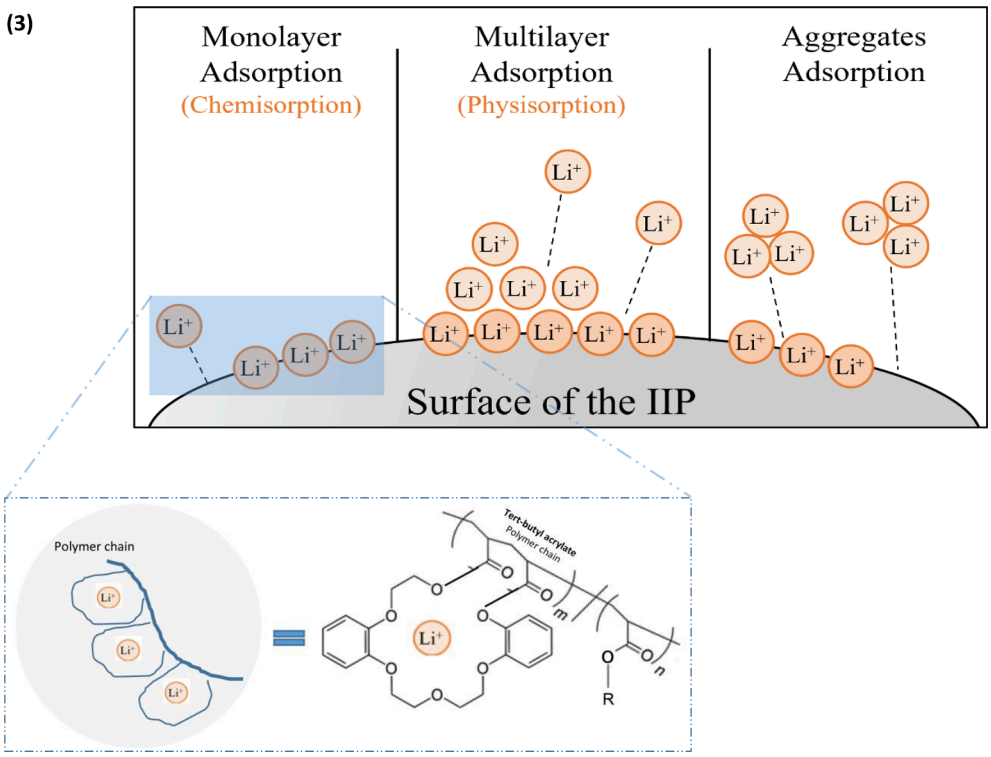

Fig. 8. (*continued*).

was following Freundlich model adsorption behavior much better than Langmuir and Temkin isotherm model behavior [49,48], While Hassanzadeh et al. [21] Cr(VI) IIP was following Temkin model, which suggests that reversible heterogeneous ion adsorption are happening on the IIP surfaces.

Moreover, Table 5 shows a compression between the Langmuir predicted maximum adsorption capacity (Q_m) of different adsorbents used for lithium recovery at 25 °C. It can be observed that the highest Q_m from the previous studies was 68 mg/g, while our adsorbent Q_m was around 714.3 mg/g, which is more than 10 times higher than the previously used adsorbents expecting to have more efficiency even at higher Li^+ concentration.

In addition, Chi-square (χ^2) tests were used based on each isotherm model's predicted adsorption capacity data compared with the experimental adsorption capacity data to further determine the best-fitted model for isotherm. The correlation coefficients (R^2) are usually used to evaluate the models' fitness for the linear regression. But, the R^2 values of Freundlich and Langmuir isotherms were very high and exactly the same (0.99), which makes the decision of the best-fitted model difficult. As a result, the Chi-square test is used to determine the best isotherm models. When the χ^2 value is smaller, this indicates that the experimental data were similar or closer to the predicted data and vice versa [4]. The Chi-square values (Table 4) shows that the Freundlich models have the lowest values over all the used temperature, indicating that the Freundlich isotherm is the best-fit model for the experimental data. This insure the previous expectation from the isotherm models that the IIP adsorption follows Freundlich model behavior with heterogeneous and multilayer adsorption.

Furthermore, based on the isotherm results, the thermodynamics were calculated at 25 °C, 35 °C, and 45 °C. Table 4 shows the values of the Gibbs free energy (ΔG°), enthalpy (ΔH°), and entropy (ΔS°) of the IIP. The thermodynamic study was performed to further understand the behavior of the adsorption process with the changes in the temperatures. The ΔG° values obtained were −0.16 kJ/mol, −0.11 kJ/mol, and −0.10 kJ/mol at 25 °C, 35 °C, and 45 °C, respectively. The negative values of the Gibbs free energy indicated that the adsorption process of Li^+ onto the IIP is spontaneous and viable. Similarly, the ΔH° was −2.62 kJ /mol, where the negative value of the enthalpy indicates that the process is exothermic. This confirms that the temperature effect on the Li^+ adsorption was negligible, and the process is not affected by the increase in temperature. Lastly, the ΔS° was 0.008 J/K mol, where the positive value of the entropy indicates that the adsorption of the Li^+ adsorption onto the IIP was favorable, and the process takes place with increased randomness and disorder. Similar results were obtained by Wahib et al. [46], where the thermodynamics study of the adsorption of Li^+ from

Table 4
Li^+ Adsorption isotherm constants, Chi-Square (χ^2), and thermodynamics of IIP under different temperatures (25 °C, 35 °C, and 45 °C).

Model	Langmuir	Freundlich	Temkin	D-R	Thermodynamics
25 °C	R^2 = 0.99	R^2 = 0.99	R^2 = 0.88	R^2 = 0.89	ΔG°= −0.16 kJ/mol
	Q_m = 714.3	n = 0.97	A_t = 4.08	q_s = 206.44	ΔH°= −2.62 kJ /mol
	b = 1.109	K_f = 89.14	B_t = 26.08	K = -0.0009	ΔS°= 0.008 J/k mol
	χ^2 = 184.58	χ^2 = 1.70	χ^2 = 42.26	–	
35 °C	R^2 = 0.99	R^2 = 0.99	R^2 = 0.89	R^2 = 0.85	ΔG°= −0.11 kJ /mol
	Q_m = 2000	n = 0.98	A_t = 4.26	q_s = 198.34	ΔH°= −2.62 kJ /mol
	b = 1.044	K_f = 93.80	B_t = 26.90	K = -0.0009	ΔS°= 0.008 J/k mol
	χ^2 = 63.47	χ^2 = 9.03	χ^2 = 62.24	–	
45 °C	R^2 = 0.99	R^2 = 0.99	R^2 = 0.88	R^2 = 0.88	ΔG°= −0.10 kJ /mol
	Q_m = 2500	n = 0.99	A_t = 4.61	q_s = 202.35	ΔH°= −2.62 kJ /mol
	b = 1.037	K_f = 97.55	B_t = 28.46	K = -0.0009	ΔS°= 0.008 J/k mol
	χ^2 = 19.68	χ^2 = 1.08	χ^2 = 43.75	–	

Table 5
Maximum adsorption capacity of different adsorbents used for lithium recovery.

Adsorbent	Lithium solution type	Maximum adsorption capacity (mg/g) (Langmuir equation), 25 °C	Reference
Lithium ion-imprinted polymer	SWRO brine	714.3	Current study
Roasted modified date pits	SWRO brine	17.86	[1]
Ferrocyanide modified date pits	SWRO brine	4.97	[1]
Porous fiber-supported lithium ion-sieve	Geothermal water	30.51	[54]
Iron-doped titanium lithium ionsieves	Brine	39.8	[47]
Date pitsimpregnated with ionic liquid	Groundwater	8.7	[46]
Date pits	Groundwater	68.0	[46]

groundwater using date pits impregnated with cellulose nanocrystals and ionic liquid. Their results showed that ΔG° and ΔH° were negative, indicating that the adsorption process was spontaneous and exothermic and is not affected by temperature, while ΔS° was negative indicating that they do not favor the increased randomness and disorder.

Fig. 8(3) shows the different possible adsorption mechanisms for IIP. If a chemisorption mechanism toke place, this will result in monolayer adsorption, which describes the Langmuir model behavior. This mechanism needs a chemical bond between the adsorbate and the adsorbent surface, and it is a naturally irreversible mechanism. However, if a physisorption mechanism took, this will result in multilayer adsorption, which describes the Freundlich model behavior. This mechanism involves weak Van der Waal forces, and it is a naturally reversible mechanism. The third adsorption mechanism is aggregates adsorption, wherein this mechanism there is a particle–particle interaction between the adsorbate themselves and particle–surface interaction between the adsorbent and the adsorbate.

3.6. Desorption recovery and Desorption-Adsorption study

The ions adsorbed on the used IIP from the previous isotherm experiments were desorbed by leaching using 0.5 mol/L HNO_3 to evaluate the possibility to recover ions from the IIP. Fig. 9 shows the recovered ions % that was adsorbed on the IIP. The Li^+ desorption results (Fig. 9A) show that 94.03% − 94.71% of the ions were recovered, while the Sr^{2+} desorption results (Fig. 9B) show that 96.35% − 96.56% of the ions was recovered. It can be observed that strontium recovery is higher than lithium recovery. This could be due to many reasons, one of them is the low adsorbed concentration of strontium initially, which makes the desorption process more efficient to leach all of the ions. Another reason is that the IIP is designed to selectively adsorb Li^+, this could make the binding of the ions to the IIP stronger, which needs a higher force to leach them. Alternatively, it may be that some IIP was already lost to the filters while filtering the adsorption solution before or while drying the filters, which means that some ions were direct, lost with the IIP. Overall, the recovered percentage is considered high for both Li^+ and Sr^{2+}. In an experiment that was done by Al-Ajji and Al-Ghouti [2], hazelnut shell adsorbent and nano-adsorbents were repeatedly used and desorbed 3 times, and the average recovery percentage was about 88% and 71% respectively. This result suggested that the adsorbents are reusable efficiently.

To assess the reusability and the IIP stability, the polymer was reused again to adsorb Li^+ in a second cycle after the desorption process, as the regeneration of the IIP is a significant characteristic to consider adsorbent as economic and eco-friendly.

Fig. 9C shows the IIP regeneration performance using different initial Li^+ concentrations (5, 15, 30, 45, 60, 75, 90, and 100 mg/L) at 25 °C and pH10. The results show the adsorption capacity of two adsorption–desorption cycles, it can be observed that the difference between cycle 1 adsorption capacity and cycle 2 adsorption capacity decreased between 1.37% and 1.54%. It is also noticed that as the Li^+ initial concentration increased, the difference between the adsorption capacities increased. This could be a result of fewer binding sites available when the concentration of ions is higher. Overall, the results suggest that the IIP can be reused successfully with high adsorption efficiency, which indicates that even after multiple uses; the IIP upholds a memory effect and strong structure [23].

An ion-imprinted microporous membrane to adsorb lithium was prepared by Sun et al. [44], and it was used for 6 times adsorption–desorption experiments to evaluate the regeneration performance. A decrease of 9.09% of the adsorption capacity was observed, and this percentage concluded that the ion-imprinted membrane was stable and had high regeneration performance. Huang and Wang's [22] IIP for lithium recovery was also run for 10 adsorption–desorption cycles, and the adsorption capacity difference between the first and the tenth cycle was decreased by 13.1%, indicating that the IIP can be used even more than 10 times with high efficiency to adsorb Li^+.

3.7. Real brine batch adsorption

After characterizing the IIP and evaluating its performance using the synthetic ionic solution, the IIP was used on real SWRO brine at 25 °C and pH 10. The efficiency of IIP to adsorb lithium and strontium from brine is shown in Fig. 10A, where the adsorption removal% of Li^+ was between 84.21% and 84.68%, while the adsorption removal% of Sr^{2+} was between 3.83% and 10%. It can be noticed that the removal% of Li^+ in brine was less by around 15% compared with the removal% of Li^+ from the synthetic solution (Fig. 7A), as well, the Sr^{2+} removal% from brine is less compared with that from the synthetic solution (Fig. 7B). This indicates that the ionic complexity of the solution affects the IIP performance. This could be due to the increased competition on the binding sites, and the extremely high salinity of the brine. Moreover, it should be taken to account that the ions in the brine are electrostatically bonding to each other with intermolecular forces, which increases the difficulty for single Li^+ to be adsorbed to the binding sites, unlike the synthetic solution that was prepared with LiCl just like the IIP templet, which was prepared using LiCl.

Looking at the adsorption capacity of the IIP (Fig. 10B), it can be observed that Qe is higher when the brine is more concentrated and decreased as it is diluted. This IIP behavior is compatible with the previous results of the synthetic solution (Fig. 7A) and with the results of Luo et al. [31] IIP used for Li^+ recovery from wastewater, where the Qe was rising as the Li^+ concentration increased until it reaches a concentration around 700 mg/L and it gets saturated. Likewise, the correlation between the IIP adsorption capacity and equilibrium concentration of Li^+ (Fig. 10C) was a positive linear correlation, while the correlation for Sr^{2+} (Fig. 10D) was a random correlation without any consistency. This ensures that the IIP Qe is highly affected by the ions concentration of the ion that the IIP was prepared to selectively adsorb.

3.8. Statistical analysis

Statistical analysis was employed to investigate the significance of the different factors and the correlation between them. Minitab statistic program was used to generate all of the results in this section. Table 6 shows the factors information that was used to calculate the analysis of variance (ANOVA) of Qe versus Temperature and Concentration for both Li^+ and Sr^{2+} adsorption isotherm experiments. The ANOVA test is used to check the significance of the factor effect by checking the P (probability) value. P-values less than 0.01, less than 0.05, or greater than 0.05 indicate that the factor is highly significant, significant, or not significant, respectively. The ANOVA (Table 6) of the Li^+ adsorption

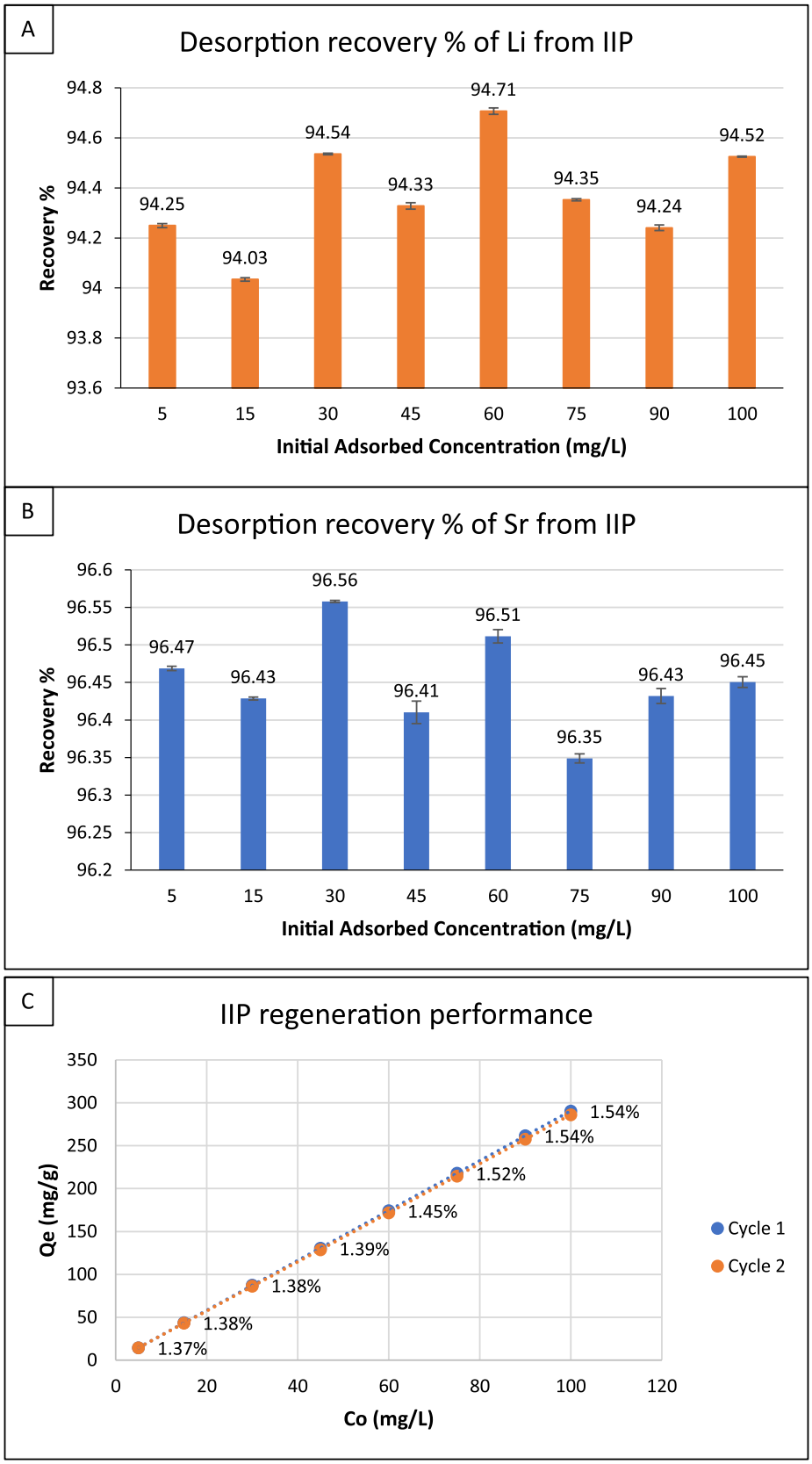

Fig. 9. IIP ions desorption recovery efficiency of (A) Lithium, and (B) Strontium, at 25 °C. And (C) IIP regeneration performance of 2 adsorption–desorption cycles at 25 °C and pH10.

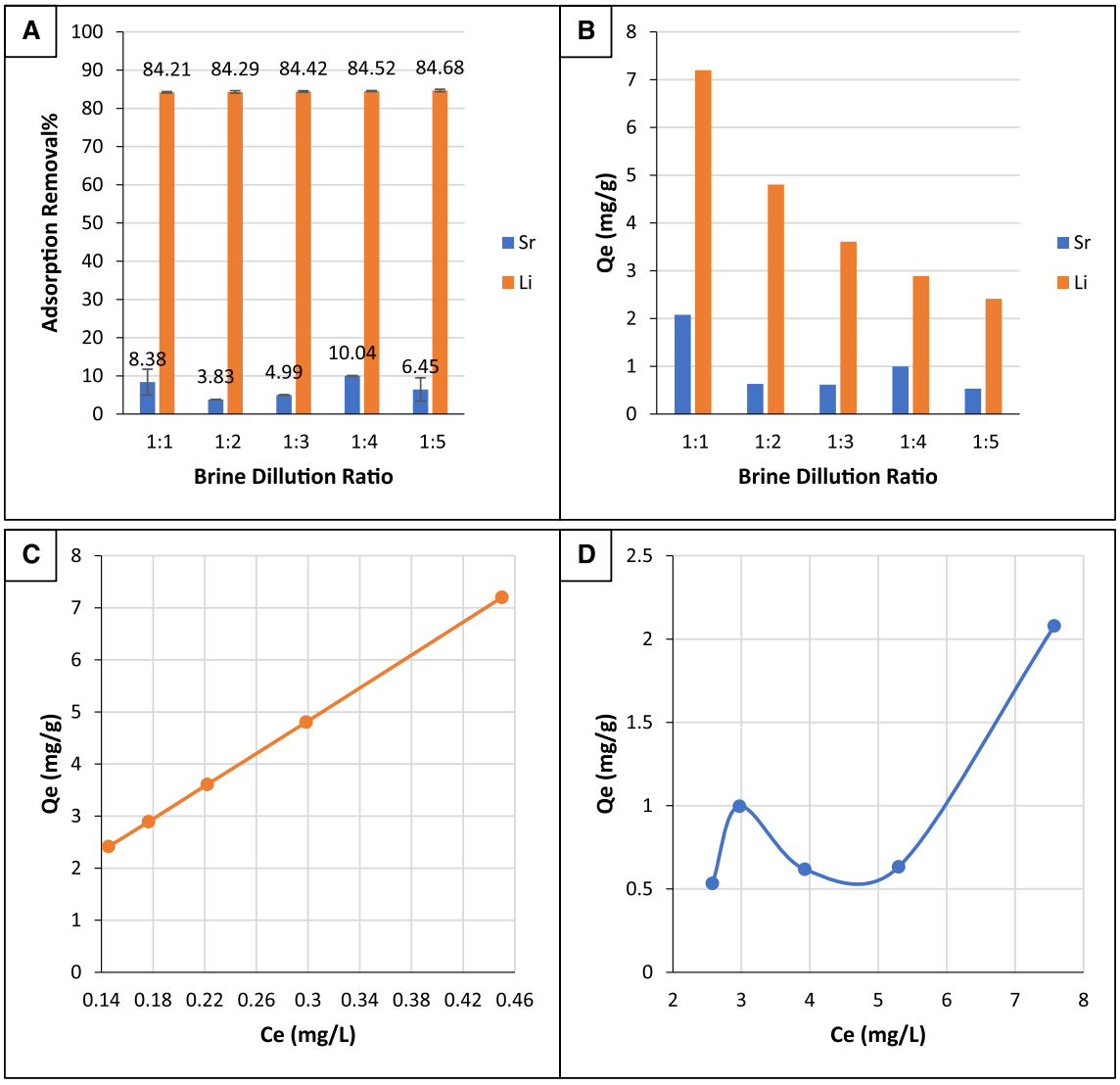

Fig. 10. (A) IIP adsorption removal%, and (B) Adsorption capacity of the IIP toward lithium and strontium from SWRO brine using different brine: distilled water dilution ratios at 25 °C and pH10. And the correlation between the IIP adsorption capacity and equilibrium concentration of (C) Lithium and (D) Strontium from SWRO brine.

experiment shows that the temperature p-value = 0.092, which indicates that it is not a significant factor, while concentration was a highly significant factor with a P-value = 0, additionally, the two factors combined had a P-value = 0.024; indicating a significant effect. This was expected from the experimental results, as it was shown that as the temperature changes, there was no difference in the adsorption capacity, while in the case of initial concentration changes, the adsorption capacity was in a direct correlation with the changes. On the other hand, the Sr^{2+} adsorption experiment shows that all the factors have a P-value = 0, which statistically indicates that the factors are significant. However, this result is not realistic, as it was shown that the Sr^{2+} adsorption experiment was showing random results with a huge difference and no regular trend with changes in the factors, which means that this outcome was not due to the factors' significant effect.

Furthermore, Tukey pairwise comparisons were used to compare the Qe means versus temperature and concentration in the grouping method depending on the significant difference in the means. Table 6 shows the Li^{+} adsorption experiment means grouping information, it can be noticed clearly that each initial concentration from the different temperatures shares the same group (same letter). Which again insure that the concentration is a significant factor while temperature did not affect the means. On the other side, the Sr^{2+} adsorption experiment means grouping information did not show any specific trend behind the grouping distribution. For example, means sharing group B are from 5 different initial concentrations of Sr^{2+} (30, 45, 60, 90, and 100 mg/L) and the different three temperatures used (25 °C, 35 °C, and 45 °C). This indicates clearly that the significance was totally due to randomness in the adsorption not due to factors effect.

Moreover, factorial plots for Qe were generated as the main factors plot and interaction plot for both Li^{+} and Sr^{2+} adsorption isotherm experiment. The main factor plot shows the effect of each factor on the Qe separately, while the interaction plot shows the effect of the interaction of the different factors together on the Qe. The results of this factorial plot are just additional evidence to assure the previous outcomes. Fig. 11 shows the factorial plots of the adsorption experiment for Qe, where the main factors plot of Li^{+} (Fig. 11A) shows that temperature alone has no significant effect on the mean of Qe, while concentration alone has a significant effect on the mean of Qe as it shows a direct proportion. The interaction plot (Fig. 11C) shows the effect on the mean of Qe when the two factors combine. It is clearly observed that the mean of Qe is increasing as the concentration increases despite the temperature changes. On the other hand, the factorial plots of the Sr^{2+}

Table 6
Analysis of Variance (ANOVA) and grouping information using the Tukey method and 95% confidence for the adsorption experiment.

Factor	Type	Levels	Values		
Temperature	Fixed	3	25, 35, 45		
Concentration	Fixed	8	5, 15, 30, 45, 60, 75, 90, 100		
Source	**DF**	**Adj SS**	**Adj MS**	**F-Value**	**P-Value**
Li^+ adsorption experiment					
Temperature	2	1	0.5	2.64	0.092
Concentration	7	427,896	61128.1	353062.25	0.000**
Temp. × Conc.	14	6	0.4	2.48	0.024*
Error	24	4	0.2		
Total	47	427,908			
Sr^{2+} adsorption experiment					
Temperature	2	4049	2024.52	39.97	0.000**
Concentration	7	12,253	1750.42	34.56	0.000**
Temp. × Conc.	14	9218	658.42	13.00	0.000**
Error	24	1216	50.65		
Total	47	26,735			

Grouping information using the Tukey method

Tukey method for Li^+ adsorption experiment

Temp.*Conc.	N	Mean	Grouping
45 100	2	291.000	A
25 100	2	290.400	A
35 100	2	288.990	A
35 90	2	261.792	B
25 90	2	261.670	B
45 90	2	261.643	B
35 75	2	218.554	C
45 75	2	218.430	C
25 75	2	217.800	C
35 60	2	175.131	D
45 60	2	174.807	D
25 60	2	174.222	D
35 45	2	131.328	E
45 45	2	131.112	E
25 45	2	130.396	E
35 30	2	87.448	F
45 30	2	87.345	F
25 30	2	87.269	F
45 15	2	43.646	G
25 15	2	43.612	G
35 15	2	43.295	G
45 5	2	14.534	H
35 5	2	14.509	H
25 5	2	14.446	H

Tukey method for Sr^{2+} adsorption experiment

Temp.*Conc.	N	Mean	Grouping					
35 90	2	92.8800	A					
35 60	2	67.0500	A	B				
35 30	2	49.0050		B	C			
45 90	2	44.8200		B	C	D		
25 100	2	43.9500		B	C	D	E	
35 45	2	43.7400		B	C	D	E	
25 90	2	33.2100			C	D	E	F
25 60	2	19.3500				D	E	F G
45 30	2	16.4700				D	E	F G
45 75	2	15.9750				D	E	F G
45 60	2	15.1200					E	F G
25 75	2	14.6250						F G
35 100	2	11.1000						F G
25 30	2	10.6200						F G
35 15	2	10.4625						F G
45 15	2	8.3250						F G
25 15	2	7.5600						F G
45 100	2	6.4500						F G
25 5	2	4.6725						F G
35 5	2	4.1475						G
45 5	2	3.0900						G
25 45	2	2.6325						G
45 45	2	2.4975						G
35 75	2	0.7875						G

-* Significant, ** Highly significant.
-Means that do not share a letter are significantly different.

adsorption experiment for Qe, where the main factors plot (Fig. 11B) shows a fluctuation in the effect of concentration on the mean of Qe, while the temperature effect shows that at 35 °C the mean of Qe highly improved. Comparing it with the interaction plot (Fig. 11D), it is obviously observed that 35 °C was not a really favorable temperature to improve the Qe, as there are higher, lower, and equal values with the other used temperatures. It is again indicating that the factors are not affecting the adsorption of strontium, but the only effect is the ion itself, as the IIP was prepared to selectively adsorb lithium only.

3.9. Cost analysis

As a cost-effective adsorbent, it is necessary to determine the IIP preparation overall cost in order to study the feasibility of the adsorbent, assist in the decision making, optimize the procedures, and predict the economic aspect. Moreover, the cost analysis help in further improvement for better preparation process feasibility. The cost analysis (Table 7) of the prepared IIP was done based on a laboratory. The results show that the total cost to prepare 3 g of IIP is around 6 USD. This amount was enough to carry out all of the experiments of this study (less than 1 g), the pure samples that were given for IIP characterization, with more than half of it as a leftover.

4. Conclusion

In conclusion, this study was undertaken to design a strategy for a major environmental concern, which is brine water and evaluate its efficiency. A novel tailored ion-imprinted polymer was successfully synthesized by polymerization technique for selective adsorption of lithium ions from reverse osmosis brine, as a cost-efficient and ecologically beneficial adsorbent to extract metals from brine. The prepared polymer was tested to adsorb lithium ions as well as strontium ions to try the selectivity of the IIP. The IIP was prepared using a Li^+ template and used under different pH values, initial concentrations, and temperatures, to optimize the experimental conditions, with the verification of the optimum temperature by RSM. It was indicated that Li^+ adsorption is not affected by changing the pH or the temperature, and only the initial concentration matters. The Sr^{2+} adsorption was random with no obvious trend toward the different factors, so the experiments were optimized to room temperature and pH 10 as it was the best for Sr^{2+} adsorption. The IIP was then characterized before adsorption compared to after adsorption of Li^+ and Sr^{2+} using SEM, TEM, FTIR, XRD, BET, EDX, and XPS, to study morphology, functional groups, specific surface area, pore radius, elemental composition, and to quantify the surface composition of the polymer. It was shown that the IIP was successfully synthesized with excellent efficiency to adsorb Li^+ but not Sr^{2+}, and it was following the Freundlich isotherm model behavior which was further insured using the Chi-Square test, and the thermodynamics study revealed that the adsorption of Li^+ on the IIP favored exothermic conditions. The used IIP was subjected to a desorption experiment and showed efficient ion recovery% for both adsorbed ions, and a cycle of the adsorption–desorption process was done that evaluated an efficient regeneration performance of the IIP. Seawater reverse osmosis brine was physically and chemically characterized and used as the real sample for ion adsorption. The results also showed a good indicator for Li^+ adsorption removal%, unlike Sr^{2+} adsorption removal%. Li^+ adsorption capacity and the correlation between adsorption capacity and equilibrium concentration were directly proportional for both the synthesized Li^+ solution experiment and the real brine. Statistical analysis was done using Minitab to generate ANOVA, Tukey pairwise comparison, and factorial plot, which complied with the previous outcomes, ensuring the reliability of the results of the experiment. Cost analysis was done for the overall price of synthesis IIP, it was concluded that it cost 6 USD to prepare 3 g of IIP, which was enough to conduct the whole experiment and characterization with a leftover.

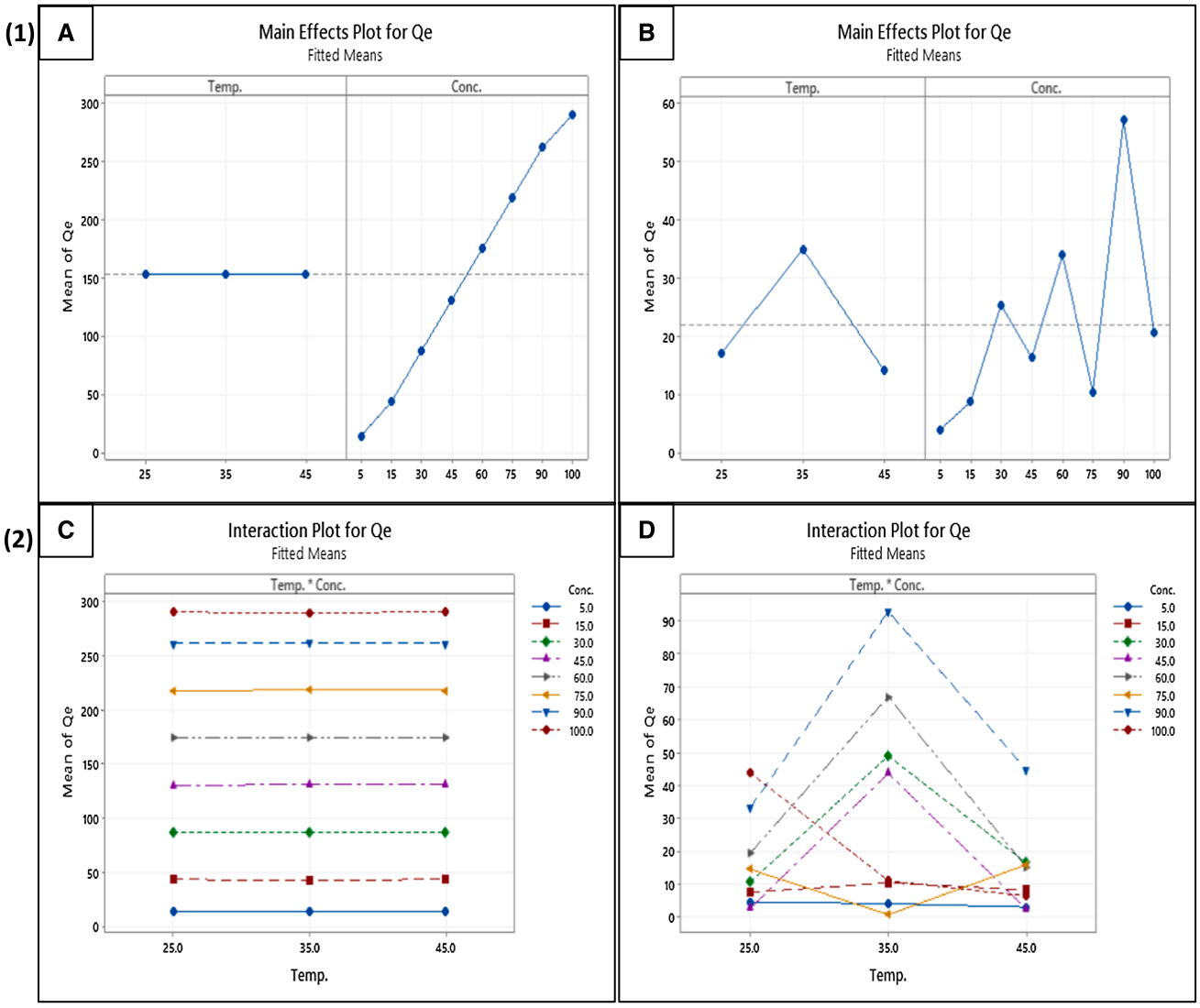

Fig. 11. Factorial plots of adsorption experiment for Qe (1) Main factors plot of (A) Li^{+} and (B) Sr^{2+}, and (2) Interaction plots of (C) Li^{+} and (D) Sr^{2+}.

Table 7
total cost required for the preparation of IIP.

Item	Unit cost (USD)	Amount used	Cost (USD)
Acetonitrile (2.5 L)	29.43	20 mL	0.24
Lithium chloride (500 g)	119.84	21.28 mg	0.0051
Potassium persulfate (500 g)	8.55	25 mg	0.00043
Ethylene glycol dimethacrylate (500 g)	194.97	792.9 mg	0.31
Dicyclohexano-18-crown-6 (100 g)	1300	74.5 mg	0.97
Tert-butyl acrylate (1 kg)	145.27	128.17 mg	3.72
Cost of polymerization heat and drying	0.036 per kWh	5.88 kWh (65C, 24 h), (Energy to Heat at 65C = 0.245 kWh/hr)	0.21
Net cost			5.45
Other overhead costs (10% of the net cost)			0.55
Total cost			6

CRediT authorship contribution statement

Sara M. Alshuiael: Formal analysis, Methodology, Validation, Writing – review & editing. **Mohammad A. Al-Ghouti:** Conceptualization, Supervision, Visualization, Formal analysis, Methodology, Validation, Writing – review & editing.

Declaration of Competing Interest

The authors declare that they have no known competing financial interests or personal relationships that could have appeared to influence the work reported in this paper.

Acknowledgment

This work was made possible by Qatar University collaborative internal grant [QUCG-CAS-20/21-2]. The findings achieved herein are solely the responsibility of the author[s]. The ICP-MS, SEM, and TEM were accomplished in the Central Laboratories Unit, Qatar University. XRD was accomplished in the Center of Advanced Materials, Qatar University. XPS was accomplished in the Gas Processing Center, Qatar University. Open Access funding provided by the Qatar National Library.

References

[1] R.S. Al-Absi, M.H. Abu-Dieyeh, R. Ben-Hamadou, M.S. Nasser, M.A. Al-Ghouti, Thermodynamics, isotherms, and mechanisms studies of lithium recovery from

seawater desalination reverse osmosis brine using roasted and ferrocyanide modified date pits, Environmental Technology & Innovation 25 (2022) 102148, https://doi.org/10.1016/j.eti.2021.102148.
[2] M.A. Al-Ajji, M.A. Al-Ghouti, Novel insights into the nanoadsorption mechanisms of crystal violet using nano-hazelnut shell from aqueous solution, Journal of Water Process Engineering 44 (2021) 102354, https://doi.org/10.1016/j.jwpe.2021.102354.
[3] A. Ansori, S.A. Wibowo, H.S. Kusuma, D.S. Bhuana, M. Mahfud, Production of biodiesel from nyamplung (Calophyllum inophyllum L.) using microwave with CaO catalyst from eggshell waste: optimization of transesterification process parameters. Open, Chemistry 17 (2019) 1185–1197.
[4] M. Arshadi, M.J. Amiri, S. Mousavi, Kinetic, equilibrium and thermodynamic investigations of ni(ii), CD(II), cu(ii) and co(ii) adsorption on Barley Straw Ash, Water Resources and Industry 6 (2014) 1–17, https://doi.org/10.1016/j.wri.2014.06.001.
[5] A.A. Atia, A.M. Donia, K.Z. Elwakeel, Selective separation of mercury (II) using a synthetic resin containing amine and mercaptan as chelating groups, React. Funct. Polym. 65 (2005) (2005) 267–275.
[6] M. Behbahani, M. Taghizadeh, A. Bagheri, H. Hosseini, M. Salarian, A. Tootoonchi, A nanostructured ion-imprinted polymer for the selective extraction and preconcentration of ultra-trace quantities of nickel ions, Microchimica Acta 178 (3–4) (2012) 429–437, https://doi.org/10.1007/s00604-012-0846-x.
[7] M. Bindels, J. Carvalho, C.B. Gonzalez, N. Brand, B. Nelemans, Techno-economic assessment of Seawater Reverse Osmosis (SWRO) brine treatment with air gap membrane distillation (AGMD), Desalination 489 (2020), 114532, https://doi.org/10.1016/j.desal.2020.114532.
[8] E. Boanini, M. Gazzano, C. Nervi, M.R. Chierotti, K. Rubini, R. Gobetto, A. Bigi, Strontium and zinc substitution in β-tricalcium phosphate: An X-ray diffraction, solid state NMR and ATR-FTIR Study, Journal of Functional Biomaterials 10 (2) (2019) 20, https://doi.org/10.3390/jfb10020020.
[9] C. Branger, W. Meouche, A. Margaillan, Recent advances on ion-imprinted polymers, Reactive and Functional Polymers 73 (6) (2013) 859–875, https://doi.org/10.1016/j.reactfunctpolym.2013.03.021.
[10] Budiana I. Gusti Made Ngurah, Jasman Jasman, Neolaka Yantus A.B., Riwu Arsel A.P., Elmsellem Hicham, Darmokoesoemo Handoko, Kusuma Heri Septya, Synthesis, characterization and application of cinnamoyl C-phenylcalix[4] resorcinarene (CCPCR) for removal of Cr(III) ion from the aquatic environment, Journal of Molecular Liquids, 324, 2021, 114776.
[11] M. Cejner, R. Dobrowolski, Ion-imprinted polymers: synthesis, characterization and applications, Ann. Univ. Mariae Curie-Sklodowska, Sect. AA: Chem 70 (2015).
[12] L. Chen, X. Wang, W. Lu, X. Wu, J. Li, Molecular imprinting: perspectives and applications, Chemical Society Reviews 45 (8) (2016) 2137–2211, https://doi.org/10.1039/c6cs00061d.
[13] S. Daniel, P. Prabhakara Rao, T. Prasada Rao, Investigation of different polymerization methods on the analytical performance of palladium(ii) ion imprinted Polymer Materials, Analytica Chimica Acta 536 (1–2) (2005) 197–206, https://doi.org/10.1016/j.aca.2004.12.052.
[14] N.C. Darre, G.S. Toor, Desalination of water: A review, Current Pollution Reports 4 (2) (2018) 104–111, https://doi.org/10.1007/s40726-018-0085-9.
[15] A.M. Donia, A.A. Atia, K.Z. Elwakeel, Recovery of gold(III) and silver(I) on a chemically modified chitosan with magnetic properties, Hydrometallurgy 87 (2007) (2007) 197–206.
[16] A.M. Donia, A.A. Atia, K.Z. Elwakeel, Gold(III) recovery using synthetic chelating resins with amine, thio and amine/mercaptan functionalities, Separation and Purification Technology 42 (2) (2005) 111–116, https://doi.org/10.1016/j.seppur.2004.06.009.
[17] J. Fasihi, S. Ammari Alahyari, M. Shamsipur, H. Sharghi, A. Charkhi, Adsorption of uranyl ion onto an anthraquinone based ion-imprinted copolymer, Reactive and Functional Polymers 71 (8) (2011) 803–808, https://doi.org/10.1016/j.reactfunctpolym.2011.03.014.
[18] H. Frank, E. Rahav, E. Bar-Zeev, Short-term effects of SWRO desalination brine on benthic heterotrophic microbial communities, Desalination 417 (2017) 52–59, https://doi.org/10.1016/j.desal.2017.04.031.
[19] J.M. Gladis, T. Prasada Rao, Solid phase extractive preconcentration of uranium on to 5,7-dichloroquinoline- 8-OL modified naphthalene, Analytical Letters 35 (3) (2002) 501–515, https://doi.org/10.1081/al-120002683.
[20] B. Hashemi, M. Shamsipur, Z. Seyedzadeh, Synthesis of ion imprinted polymeric nanoparticles for selective pre-concentration and recognition of lithium ions, New Journal of Chemistry 40 (5) (2016) 4803–4809, https://doi.org/10.1039/c5nj03366g.
[21] M. Hassanzadeh, M. Ghaemy, S.M. Amininasab, Z. Shami, An effective approach for fast selective separation of cr(vi) from water by ion-imprinted polymer grafted on the electro-spun nanofibrous mat of functionalized polyacrylonitrile, Reactive and Functional Polymers 130 (2018) 70–80, https://doi.org/10.1016/j.reactfunctpolym.2018.05.013.
[22] Y. Huang, R. Wang, Highly effective and low-cost ion-imprinted polymers loaded on pretreated vermiculite for lithium recovery, Industrial & Engineering Chemistry Research 58 (27) (2019) 12216–12225, https://doi.org/10.1021/acs.iecr.9b01244.
[23] Y. Işıkver, S. Baylav, Synthesis and characterization of metal ion-imprinted polymers, Bulletin of Materials Science 41 (2) (2018), https://doi.org/10.1007/s12034-018-1578-2.
[24] M. Khan, R.S. Al-Absi, M. Khraisheh, M.A. Al-Ghouti, A better understanding of seawater reverse osmosis brine: Characterizations, uses, and energy requirements, Case Studies in Chemical and Environmental Engineering 4 (2021), 100165, https://doi.org/10.1016/j.cscee.2021.100165.
[25] E.P. Kuncoro, D.R.M. Isnadina, H. Darmokoesoemo, F. Dzembarahmatiny, O. R. Fauziah, H. Kusuma, S., Characterization, kinetic, and isotherm data for adsorption of Pb2+ from aqueous solution by adsorbent from mixture of bagasse-bentonite, Data in Brief 16 (2018) 622–629.
[26] V.V. Kusumkar, M. Galamboš, E. Viglašová, M. Daňo, J. Šmelková, Ion-imprinted polymers: Synthesis, characterization, and adsorption of radionuclides, Materials 14 (5) (2021) 1083, https://doi.org/10.3390/ma14051083.
[27] J. Lemaire, L. Svecova, F. Lagallarde, R. Laucournet, P.-X. Thivel, Lithium recovery from aqueous solution by Sorption/Desorption, Hydrometallurgy 143 (2014) 1–11, https://doi.org/10.1016/j.hydromet.2013.11.006.
[28] Z. Liu, S.K. Nalluri, J.F. Stoddart, Surveying macrocyclic chemistry: from flexible crown ethers to rigid cyclophanes, Chemical Society Reviews 46 (9) (2017) 2459–2478, https://doi.org/10.1039/c7cs00185a.
[29] P. Loganathan, G. Naidu, S. Vigneswaran, Mining valuable minerals from seawater: A critical review, Environmental Science: Water Research & Technology 3 (1) (2017) 37–53, https://doi.org/10.1039/c6ew00268d.
[30] Y.-K. Lu, X.-P. Yan, An Imprinted Organic−Inorganic Hybrid Sorbent for Selective Separation of Cadmium from Aqueous Solution, Analytical Chemistry 76 (2) (2004) 453–457, https://doi.org/10.1021/ac0347718.
[31] X. Luo, B. Guo, J. Luo, F. Deng, S. Zhang, S. Luo, J. Crittenden, Recovery of Lithium from Wastewater Using Development of Li Ion-Imprinted Polymers, ACS Sustainable Chemistry & Engineering 3 (3) (2015) 460–467, https://doi.org/10.1021/sc500659h.
[32] G. Murray, A. Jenkins, A. Bzhelyansky, O. Manuel Uy, Molecularly Imprinted Polymers for the Selective Sequestering and Sensing of Ions, JOHNS HOPKINS APL TECHNICAL DIGEST 18 (1997) 464–472.
[33] G. Naidu, S. Jeong, Y. Choi, M.H. Song, U. Oyunchuluun, S. Vigneswaran, Valuable rubidium extraction from potassium reduced seawater brine, Journal of Cleaner Production 174 (2018) 1079–1088, https://doi.org/10.1016/j.jclepro.2017.11.042.
[34] Y.A.B. Neolaka, Y. Lawa, J.N. Naat, A.A.P. Riwu, M. Iqbal, H. Darmokoesoemo, H. S. Kusuma, The adsorption of Cr(VI) from water samples using graphene oxide-magnetic (GO-Fe3O4) synthesized from natural cellulose-based graphite (kusambi wood or Schleichera oleosa): Study of kinetics, isotherms and thermodynamics, Journal of Materials Research and Technology 9 (3) (2020) 6544–6556.
[35] Y.A.B. Neolaka, G. Supriyanto, H. Darmokoesoemo, H.S. Kusuma, Characterization, kinetic, and isotherm data for Cr(VI) removal from aqueous solution by Cr(VI)-imprinted poly(4-VP-co-MMA) supported on activated Indonesia (Ende-Flores) natural zeolite structure, Data in Brief 17 (2018) 969–979.
[36] Y.A.B. Neolaka, G. Supriyanto, H. Darmokoesoemo, H.S. Kusuma, Characterization, isotherm, and thermodynamic data for selective adsorption of Cr (VI) from aqueous solution by Indonesia (Ende-Flores) natural zeolite Cr(VI)-imprinted-poly(4-VP-co-EGDMA)-ANZ (IIP-ANZ), Data in Brief 17 (2018) 1020–1029.
[37] Y.A.B. Neolaka, Y. Lawa, J. Naat, A.A.P. Riwu, Y.E. Lindu, H. Darmokoesoemo, B. A. Widyaningrum, M. Iqbal, H.S. Kusuma, Evaluation of magnetic material IIP@GO-Fe3O4 based on Kesambi Wood (Schleichera Oleosa) as a potential adsorbent for the removal of Ccr(VIvi) from Aqueous Solutions, Reactive and Functional Polymers 166 (2021), 105000, https://doi.org/10.1016/j.reactfunctpolym.2021.105000.
[38] Q.-M. Nguyen, S. Jeong, S. Lee, Characteristics of membrane foulants at different degrees of SWRO brine concentration by membrane distillation, Desalination 409 (2017) 7–20, https://doi.org/10.1016/j.desal.2017.01.007.
[39] O.S. Onwuka, N.D. Umar, O.V. Omonona, I.G. Idris, Heavy metals and rare earth elements distribution in the brine fields of awe, Keana and Giza, Central Benue Trough, Nigeria. *Journal of African Earth Sciences* 157 (2019), 103514, https://doi.org/10.1016/j.jafrearsci.2019.103514.
[40] K. Prasad, R. Kala, T. Prasada Rao, G.R.K. Naidu, Ion imprinted polymer based ion-selective electrode for the trace determination of dysprosium(iii) ions, Analytica Chimica Acta 566 (1) (2006) 69–74, https://doi.org/10.1016/j.aca.2006.02.064.
[41] T.P. Rao, R. Kala, S. Daniel, Metal ion-imprinted polymers—novel materials for selective recognition of Inorganics, Analytica Chimica Acta 578 (2) (2006) 105–116, https://doi.org/10.1016/j.aca.2006.06.065.
[42] H.S. Son, S. Soukane, J. Lee, Y. Kim, Y.-D. Kim, N. Ghaffour, Towards sustainable circular brine reclamation using seawater reverse osmosis, membrane distillation and forward osmosis hybrids: An experimental investigation, Journal of Environmental Management 293 (2021), 112836, https://doi.org/10.1016/j.jenvman.2021.112836.
[43] W.T. Stringfellow, P.F. Dobson, Technology for the recovery of lithium from geothermal brines, Energies 14 (20) (2021) 6805, https://doi.org/10.3390/en14206805.
[44] D. Sun, Y. Zhu, M. Meng, Y. Qiao, Y. Yan, C. Li, Fabrication of highly selective ion imprinted macroporous membranes with crown ether for targeted separation of lithium ion, Separation and Purification Technology 175 (2017) 19–26, https://doi.org/10.1016/j.seppur.2016.11.029.
[45] M.K. Trivedi, R.M. Tallapragada, A. Branton, D. Trivedi, G. Nayak, et al., Physical, Atomic and Thermal Properties of Biofield Treated Lithium Powder, Journal of Advanced Chemical Engineering. (2015), https://doi.org/10.4172/2090-4568.1000136.
[46] Wahib, S. A., Da'na, D. A., Zaouri, N., Hijji, Y. M., & Al-Ghouti, M. A. (2022). Adsorption and recovery of lithium ions from groundwater using date pits impregnated with cellulose nanocrystals and Ionic liquid. *Journal of Hazardous Materials*, *421*, 126657. https://doi.org/10.1016/j.jhazmat.2021.126657.
[47] S. Wang, X. Chen, Y. Zhang, Y. Zhang, S. Zheng, Lithium adsorption from brine by iron-doped titanium lithium ion sieves, Particuology 41 (2018) 40–47, https://doi.org/10.1016/j.partic.2018.02.001.

[48] X. Wang, K. Zhao, Y. Guo, L. Meng, D. Li, T. Deng, Experimental determination and thermodynamic model of solid-liquid equilibria in the ternary system (LiCl+ SrCl 2 + H 2 O) at 273.15 K and its application in industry, Journal of Solution Chemistry 48 (4) (2019) 528–545.

[49] X. Wang, K. Zhao, Y. Guo, L. Meng, D. Li, T. Deng, Experimental determination and thermodynamic model of solid–liquid equilibria in the ternary system (LiCl + srcl2 + H2O) at 273.15 K and its application in industry, Journal of Solution Chemistry 48 (4) (2019) 528–545, https://doi.org/10.1007/s10953-019-00864-4.

[50] J.-L. Xiao, S.-Y. Sun, X. Song, P. Li, J.-G. Yu, Lithium ion recovery from brine using granulated polyacrylamide–MnO 2 ion-sieve, Chemical Engineering Journal 279 (2015) 659–666, https://doi.org/10.1016/j.cej.2015.05.075.

[51] H. Xu, D. Guo, Synthesis and characterization of an ion-imprinted polymer for selective adsorption of copper ions in aqueous solution, Adsorption Science & Technology 30 (4) (2012) 293–306, https://doi.org/10.1260/0263-6174.30.4.293.

[52] Y. Yang, X. Meng, Z. Xiao, Synthesis of a surface molecular imprinting polymer based on silica and its application in the identification of nitrocellulose, RSC Advances 8 (18) (2018) 9802–9811, https://doi.org/10.1039/c7ra13264f.

[53] L. Zhao, X. Hu, F. Zi, Y. Liu, D. Hu, P. Li, H. Cheng, Preparation and adsorption properties of ni(ii) ion-imprinted polymers based on synthesized novel functional monomer, e-Polymers 21 (1) (2021) 590–605, https://doi.org/10.1515/epoly-2021-0055.

[54] Z. Zhao, H. Jiang, L. Wu, N. Yu, Z. Luo, W. Geng, Preparation of magnetic surface ion-imprinted polymer based on functionalized fe3o4 for fast and selective adsorption of cobalt ions from water, Water 14 (2) (2022) 261, https://doi.org/10.3390/w14020261.

[55] Z. Zhong, R. Rezaee, M. Josh, L. Esteban, M. Sarmadivaleh, The salinity dependence of electrical conductivity and Archie's cementation exponent in Shale Formations, Journal of Petroleum Science and Engineering 208 (2022), 109324, https://doi.org/10.1016/j.petrol.2021.109324.

[56] G. Zhu, P. Wang, P. Qi, C. Gao, Adsorption and desorption properties of Li+ on PVC-H1.6Mn1.6O4 lithium ion-sieve membrane, Chemical Engineering Journal 235 (2014) 340–348, https://doi.org/10.1016/j.cej.2013.09.068.